# 11

# HYDRODYNAMICS OF UNDULATORY PROPULSION

*GEORGE V. LAUDER*
*ERIC D. TYTELL*



## I. INTRODUCTION

In the years since publication of the major previous reviews addressing various aspects of fish undulatory propulsion (Hertel, 1966; Webb, 1975, 1978, 1993b; Aleev, 1977; Bone, 1978; Lindsey, 1978; Magnuson, 1978; Blake, 1983; Webb and Weihs, 1983; Videler, 1993), one significant new development stands out: the ability to quantify water flow patterns around swimming fishes directly. Until recently, investigations of fish propulsion have had to infer hydrodynamic function from kinematics and theoretical models. Biologists and engineers interested in how fishes interact with their fluid environment have had no quantitative way to visualize this interaction, despite the critical importance of understanding fluid flow patterns produced by swimming fishes for testing theoretical models and for understanding the hydrodynamic effects of different body and fin designs. This predicament



*Fish Biomechanics: Volume 23*
FISH PHYSIOLOGY

DOI: 10.1016/S1546-5098(05)23011-X

was well expressed by McCutchen (1977) in his chapter in the classic book *Scale Effects in Animal Locomotion* (Pedley, 1977). McCutchen (1977, p. 339) described the current state of research on fish locomotion by stating that "considering the man-hours spent studying fish propulsion, we know precious little about what the fish does to the fluid."

One early attempt to visualize the flow around swimming fishes directly was the influential master's thesis by Rosen (1959). Rosen's ingenious experiments involved swimming fish in a shallow pan of water above a thin layer of milk carefully layered on the bottom. The swimming movements of the fish disturbed the milk layer and revealed general flow patterns which Rosen then photographed. Subsequent attempts that included the use of dye or Schleiren methods (McCutchen, 1977; Arnold *et al.*, 1991; Ferry and Lauder, 1996) gave useful results but provided little information of a quantitative nature.

The combination of high-resolution high-speed video systems, high-powered continuous wave lasers, and an image analysis technique called digital particle image velocimetry (DPIV), developed over the past decade, has permitted the direct visualization of water flow over the surface and in the wake of swimming fishes (e.g., Müller *et al.*, 1997; Wolfgang *et al.*, 1999; Anderson *et al.*, 2000; Lauder, 2000; Müller *et al.*, 2001; Lauder and Drucker, 2002; Lauder *et al.*, 2003; Tytell, 2004a; Tytell and Lauder, 2004). These data have provided a wealth of new information on the fluid flows generated by the body, tail, and fins of freely swimming fishes, and represent a significant new arena of investigation not described in previous reviews.

In this chapter, we focus on recent experimental hydrodynamic data on undulatory locomotion in fishes, and provide as background a general description of the major theoretical model of undulatory propulsion. Hydrodynamic flows are caused by undulatory movements of the body and fins, and so we preface our discussion of models and experiments with an analysis of the classical kinematic modes of undulatory locomotion in fishes.

## II. CLASSICAL MODES OF UNDULATORY PROPULSION

One of the most enduring features of the literature on fish locomotion is the classification of fish swimming into general "modes" based on exemplar species (Breder, 1926; Lindsey, 1978). For example, eel locomotion is referred to as anguilliform after the eel genus *Anguilla*, and is used as shorthand for fishes that undulate large portions of their body during propulsion, generally with nearly a full wavelength present on the body at any given time (Gray, 1933; Gillis, 1996). Thunniform locomotion is based on tunas (*Thunnus*), and is verbal shorthand for fish locomotion involving a high aspect ratio tail with relatively little lateral oscillation of the body (Donley

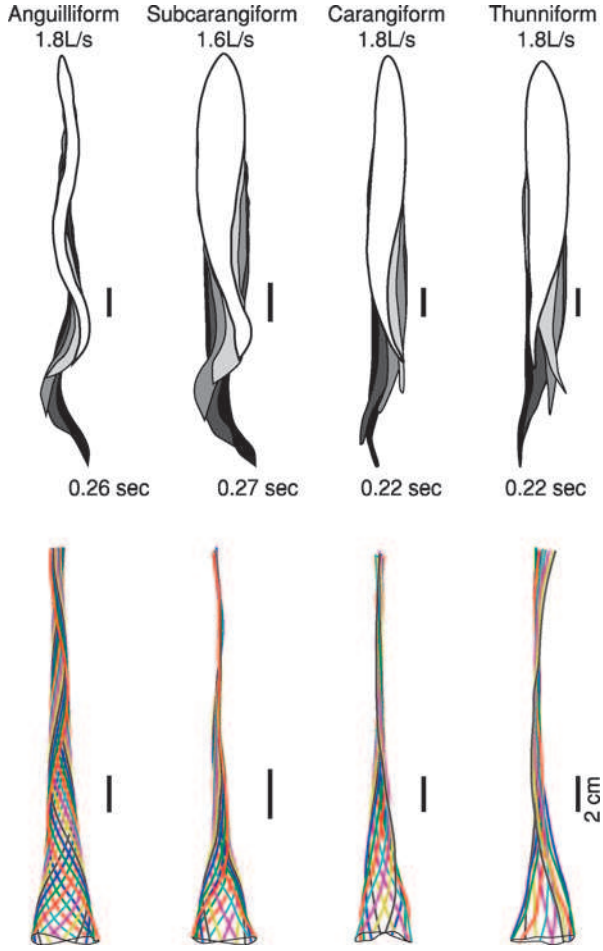


**Fig. 11.1.** Four classical categories of fish undulatory propulsion illustrated with fish outlines and midlines derived from recent experimental data. This figure updates the classical depiction presented in Lindsey (1978). Outlines of swimming fishes are shown above with displacements that to illustrate forward progression, while midlines at equally spaced time intervals throughout a tail beat are superimposed below, aligned at the tip of the snout; each time is shown in a distinct color. Anguilliform mode based on *Anguilla*, subcarangiform mode based on *Lepomis*, carangiform mode based on *Scomber*, and thunniform mode based on *Euthynnus*. All fishes were between 20 and 25 cm total length ($L$), and swam at a similar speed of 1.6 to 1.8 $Ls^{-1}$. Times shown indicate duration of the tail beat. Scale bars = 2 cm. [Fish images are based on data from Tytell and Lauder (2004), Tytell (unpublished), and Donley and Dickson (2000).]

and Dickson, 2000; Graham and Dickson, 2004). Other major categories of undulatory propulsion include carangiform locomotion (up to one half wave on the body) and subcarangiform swimming (more than one half wave but less than one full wave), although additional names have also been used for this mode (Webb, 1975; Webb and Blake, 1985; also see Chapter 7 in this volume).

While these categories endure because of their utility in describing basic patterns of locomotion and because they are easy to visualize with a simple two-dimensional analysis, they are based on older data, sometimes containing inaccuracies or obtained under unsteady swimming conditions. Perhaps the most common misconception in the current literature concerns anguilliform locomotion, as a result of Sir James Gray's classic paper (Gray, 1933), which suggested that large-amplitude undulations occur along the entire eel body at all speeds. Recent data (see data and discussion in Gillis, 1996; Lauder and Tytell, 2004; Tytell and Lauder, 2004), however, indicate that the anterior body only begins undulating at high swimming speeds and during acceleration; at lower speeds, undulation is confined to the posterior region. The eel photographed by Gray (1933) was most likely accelerating (Lauder and Tytell, 2004; Tytell, 2004b), although these images of eel locomotion are often reproduced as representing steady locomotion. Additionally, careful measurements by Donley and Dickson (2000) suggest that thunniform locomotion is not a dramatically different swimming mode, but rather a relatively modest change in the carangiform mode.

In Figure 11.1, we use recent quantitative kinematic data from the literature to produce an update to the classical illustration in Lindsey (1978) of representative modes of undulatory locomotion in fishes. The fishes illustrated in this figure all swam at similar relative speeds (1.6 to 1.8 $L s^{-1}$), were all between 20 and 25 cm in total length, and swam in a flow tank under carefully controlled conditions in which data were taken only when fishes were swimming steadily. At this moderately high sustained swimming speed of 1.8 $L s^{-1}$, there is remarkable similarity in the undulatory profiles of all four classes of locomotion. Eels show greater lateral oscillations in the front half of the body at this speed, but the amplitude envelopes from subcarangiform to thunniform are extremely similar, with nonlinear amplitude profiles that rapidly increase toward the tail and similar overall patterns of body oscillation.

The similarity becomes more pronounced at slower swimming speeds, particularly at less than 1.0 $L s^{-1}$ (Figure 11.2). A common characteristic of undulatory propulsion at low speed is that anterior body oscillations are minimal (Lauder, 2005); only when speed exceeds 1.0 $L s^{-1}$ does the front half of the body begin to oscillate laterally. For example, Figure 11.2 shows data from largemouth bass and American eels, illustrating their similarity at low speeds and the increase in lateral oscillation as speed increases (Jayne

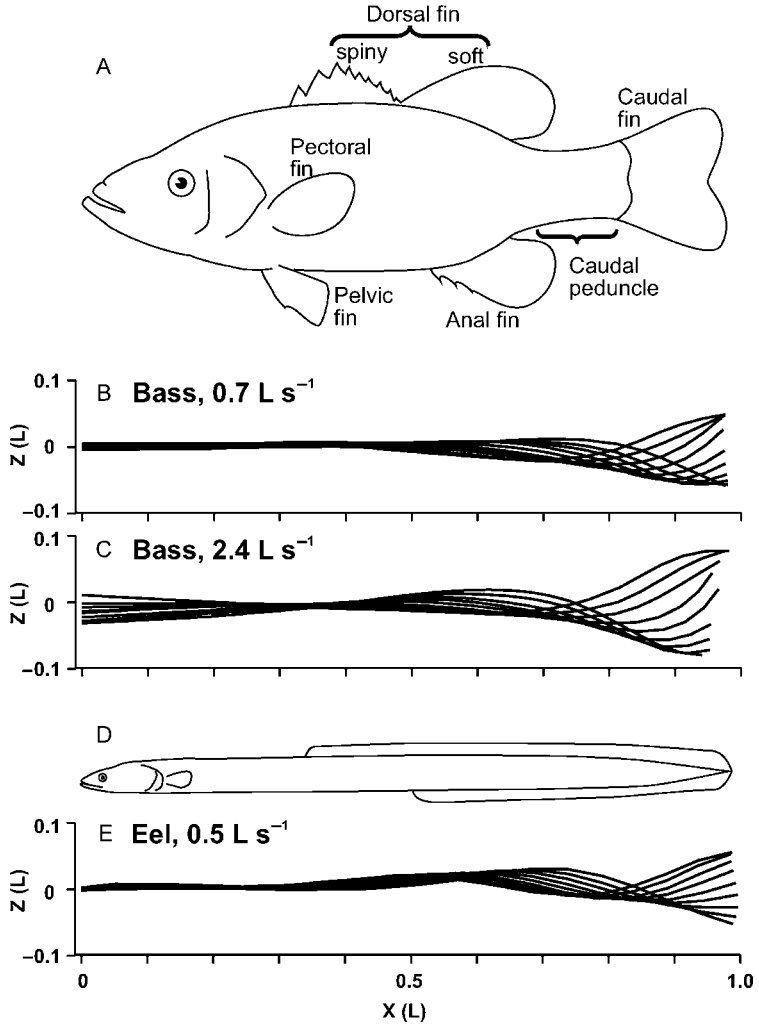


**Fig. 11.2.** (A) Outline of a largemouth bass (*Micropterus salmoides*) to illustrate the major fins and fin positions along the body and the longitudinal body profile in lateral view. (B–C) Midlines reconstructed from patterns of body bending during steady swimming in largemouth bass at speeds of 0.7 and 2.4 $Ls^{-1}$. At the slow speed, body bending is confined to the posterior half of the body, but at higher speeds the head begins to oscillate laterally. (D) Outline of an American eel (*Anguilla rostrata*) to show the contrast in body shape with the bass as seen in lateral view. (E) Reconstructed midlines of an eel swimming steadily at 0.5 $Ls^{-1}$. Note the similarity in amplitude and proportion of the body undulating for low-speed swimming in both the eel and the bass. Successive midlines in all plots are spaced equally in time during a half tail beat cycle. Z, lateral excursion in % body length ($L$); X, distance along the body, $L$. [Panels (B) and (C) modified from Jayne and Lauder (1995); panel (E) based on data from Tytell (2004a).]

and Lauder, 1995). Recruitment of increasingly anterior musculature with increased speed results in greater oscillation of the anterior body. At slow speeds, there is no anterior myotomal muscle strain, no body bending, and hence no work done in the front half of the body to power locomotion (e.g., Figure 11.2B and E).

It is our view that recent experimental data increasingly demonstrate that these taxonomically based categories do not represent important hydrodynamic differences, even though they do provide useful verbal shorthand for describing broad types of fish movement. In particular, we are concerned about two aspects of this classification scheme. First, the body amplitude profiles used to define locomotor categories, especially at slow speeds, are remarkably similar across these categories. Even fishes as different as eels and bass show very similar amplitude profiles at slow swimming speeds (Figure 11.2). Plotting midline (two-dimensional) amplitude profiles thus does little to reveal biologically significant hydrodynamic differences among species. Second, and perhaps more importantly, these categories ignore the crucial three-dimensional geometry of fishes. As illustrated in Figure 11.2A and D, most fishes possess numerous fins and regions such as the caudal peduncle that, as we discuss later, shed vortices and accelerate flow. These separation points are not visible in the two-dimensional slice through the fish midline so often used to depict locomotor modes. Many fish species have distinct tails, as well, that function like a propeller, accelerating flow and leaving a thrust signature in the wake (Lauder *et al.*, 2002; Fish and Lauder, 2005; Lauder, 2005). Another key point, which is not evident from examining standard two-dimensional depictions of fish swimming (like Figure 11.1), is that the dorsal and anal fin accelerate and redirect freestream flow; thus, the tail encounters incident flow greatly altered from the freestream (Drucker and Lauder, 2001a; Lauder and Drucker, 2004).

It is likely that the major differences in locomotor hydrodynamics among fishes are primarily a consequence of differences in their three-dimensional geometry and longitudinal area profiles, and not so much from differences in the amplitude profiles of a two-dimensional slice through the middle of the fish. In the following we present data showing a substantial hydrodynamic difference in wake structure between eels and other fish species studied to date. These differences are not attributable to midline amplitude profiles, but rather to the substantial differences in three-dimensional body shapes (Figure 11.2).

## III. THEORY OF UNDULATORY PROPULSION

Recent experimental hydrodynamic studies have all been performed in the context of several physical theories of undulatory locomotion, based on midline kinematics such as those we described previously. Although such

theories largely pass over some points that we argue are quite important, such as the three-dimensional shape of fish bodies, they provide some useful insights and an important context for the experimental studies that follow.

To begin, we approximate a fish in one of the simplest ways possible: as a flapping hydrofoil. A fish's tail, particularly that of fishes like tunas, is like a section of a hydrofoil moving from side to side. Two main parameters characterize the fluid dynamics of a flapping foil: one, Reynolds number, *Re*, describes the steady motion of the foil through the fluid; and the other, Strouhal number, *St*, describes the flapping motion.

Reynolds number is a dimensionless number that approximates the relative importance of forces due to the fluid's viscosity and forces due to the fluid's inertia. It is often written in two equivalent ways, as

$$Re = \frac{\rho UL}{\eta} \quad or \quad Re = \frac{UL}{\nu}, \tag{1}$$

where $U$ is average forward speed, $L$ is the length of the fish or the chord length of the foil, $\rho$ is the fluid density, and $\eta$ and $\nu$ are the fluid's dynamic and kinematic viscosity, respectively. The definitions of the length and speed are intentionally vague, because small differences in Reynolds number have little physical significance. Typically, only order of magnitude differences in *Re* are informative, although at certain critical points, like the transition from laminar to turbulent flow, small *Re* changes can lead to dramatic changes in the flow patterns. Nonetheless, flows are divided into three broad regimes: the viscous regime, $Re < 1$, in which viscous forces dominate; the inertial regime, $Re > 1000$, in which inertial forces dominate; and an intermediate regime between the two, in which both types of forces are important. For more information, see textbooks such as Denny (1993) or Faber (1995).

Reynolds number involves only the steady motion of the fish (or foil). Strouhal number, in turn, describes how fast the tail is flapping relative to its forward speed. It is defined as

$$St = \frac{fA}{U}, \tag{2}$$

where $f$ is the flapping frequency, $A$ is the flapping amplitude (the total distance from maximum excursion on one side to maximum excursion on the other), and $U$ is again the forward speed. Strictly speaking, *St* describes the wake behind the flapping foil, not the foil itself, but, for biological purposes, the two definitions are often used interchangeably (Triantafyllou *et al.*, 1993). Fishes, marine mammals, and even flying animals seem to flap with a Strouhal number near 0.3 (Triantafyllou *et al.*, 1993; Taylor *et al.*, 2003; Rohr and Fish, 2004), although values from close to 0 to near 1 have been reported (Horton, *et al.*, 2003; Rohr and Fish, 2004).

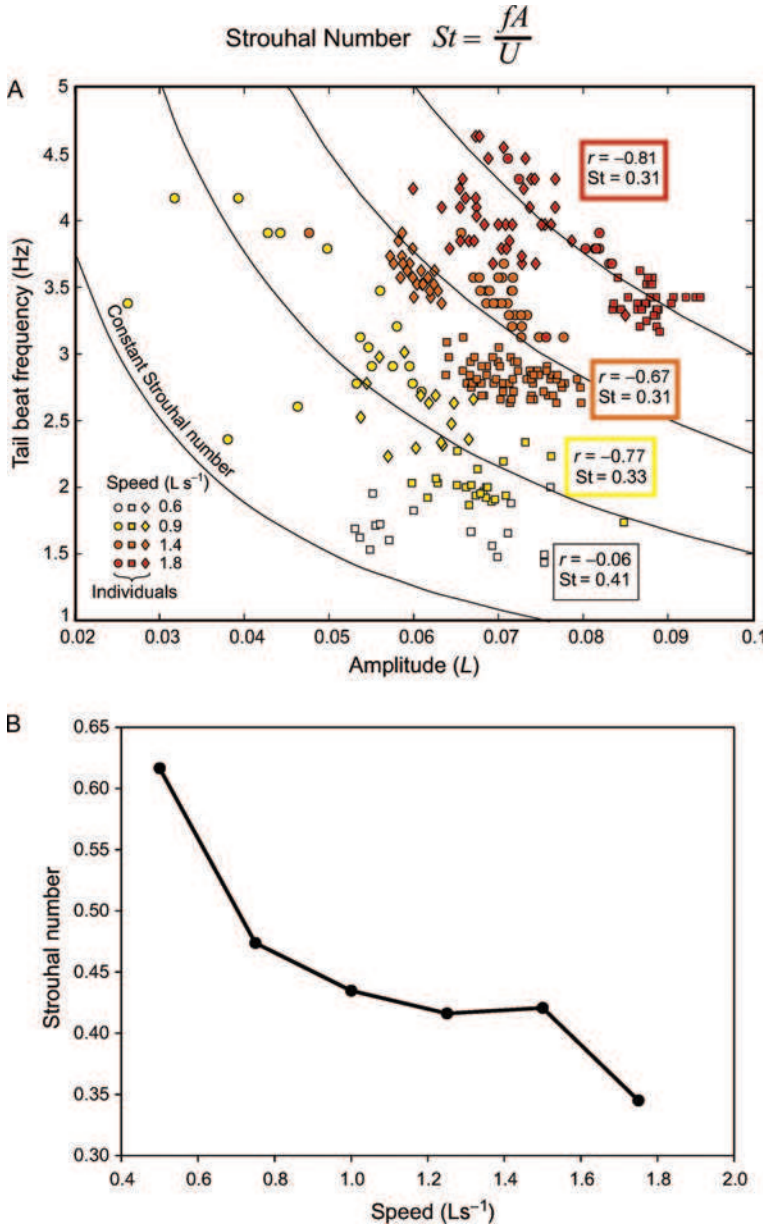
Strouhal Number $St = \frac{fA}{U}$
A
Tail beat frequency (Hz)
Amplitude (L)
Constant Strouhal number
Speed (L s$^{-1}$)
0.6
0.9
1.4
1.8
Individuals
r = –0.81
St = 0.31
r = –0.67
St = 0.31
r = –0.77
St = 0.33
r = –0.06
St = 0.41
B
Strouhal number
Speed (Ls$^{-1}$)

Figure 11.3A shows data from eels (*Anguilla*) swimming over a speed range of 0.6 to 1.8 $Ls^{-1}$; *St* for these eels varied between 0.31 and 0.41, close to the optimal flapping value predicted for swimming fishes (Triantafyllou and Triantafyllou, 1995). For a given tail (or foil) shape, experimental and theoretical studies have shown that its thrust and efficiency are strongly related to Strouhal number (Anderson *et al.*, 1998; Murray and Howle, 2003; Read *et al.*, 2003). Typically, thrust increases with increasing *St*, but efficiency peaks near 0.3 (Read *et al.*, 2003), which is the value for most swimming fishes.

However, other data show that fishes may swim with apparently non-optimal Strouhal numbers during swimming, especially at lower speeds. Figure 11.3B shows *St* for Pacific salmon (*Oncorhynchus*) swimming; at slower swimming speeds of 0.5 $Ls^{-1}$, *St* is greater than 0.6, much higher than expected for optimal thrust production. These fish may genuinely be inefficient at slow speeds, or Strouhal number may not capture the complexities of fish swimming efficiency at slow speeds.

To proceed beyond this simplistic idea of fish swimming, one must start to examine the swimming motion in more detail. The theories described in the following section treat midline kinematics as a given. In principle, these kinematics result from a complex interaction between the internal forces from muscles and the external forces from the fluid. As a fish swims, muscles deform the body, applying forces to the fluid around the body, but the fluid applies forces back on the body, changing the body shape, which changes the muscle forces, and so on. To model the body deformation accurately, both sets of forces would have to be accounted for simultaneously. Few models attempt to solve this combined problem because of its complexity (but see Ekeberg, 1993; Cortez *et al.*, 2004). Instead, most theories treat the body as a given two-dimensional shape and examine the fluid forces separately.

## A. Resistive Models

In one simple model, first proposed by Taylor (1952) and termed a ''resistive'' model, thrust is estimated from the sum of the drag forces on a

**Fig. 11.3.** Strouhal number and fish locomotion. (A) Tail-beat frequency versus amplitude at a variety of different swimming speeds for eel (*Anguilla*) locomotion; curves indicate a constant Strouhal number of 0.3, and colored symbols from white to red indicate increasing locomotor speed. Note the relative constancy of Strouhal number for eels swimming both over this speed range and within speeds. (B) Data for swimming Pacific salmon (*Oncorhynchus*) over a speed range of 0.5 to nearly 1.8 $Ls^{-1}$. Note the substantial increase in Strouhal number at slow swimming speeds. [Panel (A) modified from Tytell (2004a); data plotted in panel (B) courtesy of Jacquan Horton, Adam Summers, and Eliot Drucker.]

body with a wave traveling backward at a speed $V$ greater than its forward swimming motion $U$. The body is divided into many segments down its length, and the drag forces from each segment are summed based on the equation

$$D = \frac{1}{2} C_D \rho S u^2, \tag{3}$$

where $C_D$ is the drag coefficient, a measure of how "draggy" the segment is, $\rho$ is the fluid density, $S$ is an area, typically the presented area or the surface area of the segment, and $u$ is the segment's velocity, including contributions from both the fish's forward motion and its lateral undulations. Typically, $D$ must be broken into components perpendicular and parallel to the body, because $C_D$ differs in different directions. Finding the total force is a somewhat lengthy but mostly geometric exercise of identifying all of the segment angles. The model suffers from other substantial problems, though, most notably because Eq. (3) is valid for steady motions, but may not hold for undulatory motion, because the model assumes that anterior segments do not affect flow as fluid moves past the body, and because estimating $C_D$ can be difficult. Webb (1975) discusses the problems with resistive models in more detail.

Although this model is limited in its ability to estimate resistive forces, this is not to say that these types of forces are unimportant. They may play a role in generating thrust (Tytell, 2004a) and they may contribute to reducing propulsive efficiency (Webb, 1975).

## B. Reactive Models

The preferred analytical model of fish swimming is Sir James Lighthill's elongated body theory (1960, 1971), which is based on adding up the forces due to the lateral acceleration and deceleration of the body as it undulates from side to side. This model is often termed "reactive," because it estimates forces based on the acceleration reaction, an effect in which fluids resist changes in velocity of a moving body, as if the body had additional, "virtual," mass (Batchelor, 1973; Childress, 1981; Daniel, 1984). Other forces that could contribute to thrust, including those resulting from the fluid's viscosity, are assumed to be negligible. The following explanation closely follows that of Lighthill (1969) and Webb (1975).

Lighthill (1960) estimated force and power by adding up changes in energy. Without viscosity, there are only three places energy changes while a fish swims (Figure 11.4). First, the total energy added to the system comes from the fish's movements. This energy is consumed in two ways: (1) pushing the fish forward (thrust power) and (2) creating the wake (wake power).

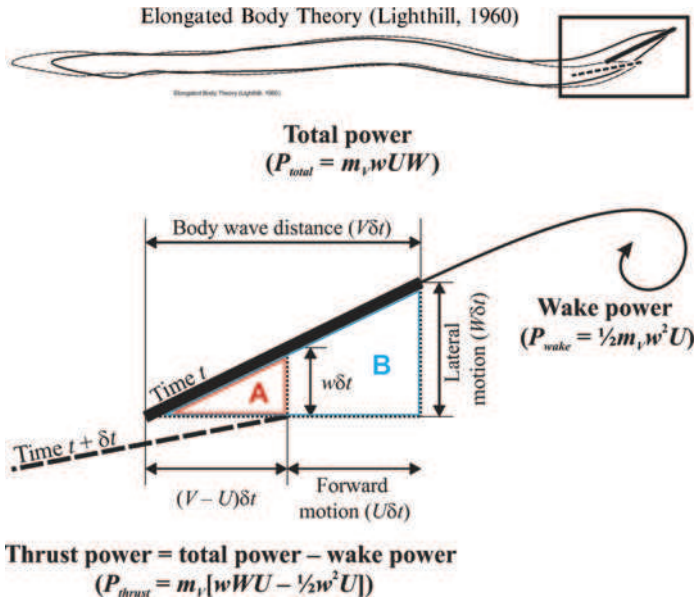


**Fig. 11.4.** Schematic view of Lighthill's (1960) reactive model showing the geometrical argument used to derive average thrust power. Top: Outlines of an eel at two different points in time (indicated by solid and dashed lines). The tail region is outlined with a box and enlarged below. Bottom: Enlarged view of tail tip segments at two points in time, showing geometrical parameters and the three components of energy in the system (bold equations). The two similar triangles used in the analysis (A and B) are outlined in red and blue, respectively. Total power added to the system, shown at the top, is consumed generating the wake, at right, and propelling the fish forward, at bottom. This figure is discussed in detail in the text. (After Webb, 1975.)

Energy has to be conserved, so these changes in energy must add up to zero. Thus, recalling that power is the rate of change of energy,

$$(\text{total undulatory power}) - (\text{thrust power}) - (\text{wake power}) = 0 \qquad (4)$$

If we average these changes in energy over a tail-beat cycle, we can express their mean values based on a geometrical argument examining only the tail's motion. Because undulation is symmetric, the side-to-side motion of the body produces forces that average out over a tail beat. Only the tip of the tail is different: when it changes the fluid's momentum, that momentum is shed into the wake. Thus, to determine average thrust and power, we can restrict our analysis to the tail tip.

First, we examine the tail's motion. The segment at the tip of the tail moves forward and laterally during a time period $\delta t$ (Figure 11.4). We define

the length of the segment (projected on the swimming direction) to be $V\delta t$, where $V$ is the speed of the body wave. During the time interval, the segment moves forward a distance $U\delta t$ and laterally a distance $W\delta t$, where $U$ is the forward swimming speed and $W$ is the lateral velocity of the tail tip. The water, however, is pushed laterally over a smaller distance $w\delta t$, because of how the forward and lateral motions combine (Figure 11.4). This velocity $w$ approximates the motion of the tail segment perpendicular to itself, assuming that the tail does not make a large angle to the swimming direction. The difference between $w$, the velocity that actually affects the fluid, and the lateral tail velocity $W$ is related to the difference in the body wave speed $V$ and the swimming speed $U$. If the fish were pinned in place, such that $U$ were zero, all of the lateral motion would affect the fluid and $w$ would equal $W$. But if $U$ and $V$ were the same, then the tail tip would slip exactly into the spot just vacated by an upstream segment and the fluid would see no lateral motion at all.

To derive $w$, we examine the two similar triangles **A** and **B** in Figure 11.4:

$$\frac{w\delta t}{W\delta t} = \frac{(V-U)\delta t}{V\delta t} \tag{5}$$

or

$$w = W\frac{V-U}{V}, \tag{6}$$

which is, as we expected, less than $W$. Because $w$ is the lateral velocity the fluid encounters, the tail increases the lateral momentum of the fluid by $m_V w$, where $m_V$ is the virtual mass per unit length at the tail tip. This momentum is shed off the tail tip into the wake at the same rate the fish swims forward, $U$, and the tail itself does work on it as it moves laterally at a rate $W$. Thus, the total power is

$$P_{\text{total}} = m_V w U W. \tag{7}$$

As discussed previously, this input power is divided up into two outputs: the thrust power and the power to create the wake. The wake power is the kinetic energy of the fluid shed into the wake at speed $U$,

$$P_{\text{wake}} = \frac{1}{2} m_V w^2 U. \tag{8}$$

Subtracting the wake power (8) from the total power (7), according to the energy balance (4), we arrive at the average thrust power:

$$P_{\text{thrust}} = m_V(wWU - \frac{1}{2}w^2U). \tag{9}$$

Because power is force multiplied by velocity, we can also write the average thrust force $F_{\text{thrust}}$ as $P_{\text{thrust}} / U$.

The virtual mass per unit length $m_V$ is fairly well approximated by the density of water $\rho$ multiplied by the area of the circle that circumscribes the tail tip, including any fins sticking off (Lighthill, 1970). Thus,

$$m_V = \frac{1}{4}\pi\rho d^2, \tag{10}$$

where $d$ is the dorso-ventral height of the caudal fin at the trailing edge.

We can gain some insight into Eq. (9) if we assume that the body has a simple, constant amplitude traveling wave. Averaged over the tail beat period, we find that mean thrust $F_{\text{thrust}}$ is proportional to $V^2$–$U^2$. Thus we return to Gray's (1933) observation: for positive thrust, the body wave speed should be faster and in the opposite direction as the swimming speed. In fact, to maximize thrust, body wave speed should be as large as possible.

The reason why fish do not use the largest body wave speed possible becomes clear if we calculate efficiency. The Froude propulsive efficiency $\eta$ is the ratio of useful (thrust) power to total power, or

$$\eta = \frac{P_{\text{thrust}}}{P_{\text{total}}} = 1 - \frac{1}{2}\frac{V - U}{V}, \tag{11}$$

based on Eqs. (6)–(9). Maximum efficiency is achieved when body wave speed is equal to the swimming speed. Clearly, fishes are faced with a tradeoff. At maximum efficiency, thrust is zero, and at high thrust, efficiency is low. Note that the efficiency cannot possibly be lower than 0.5, however, according to Eq. (11).

The reactive model described previously makes the assumption that undulatory amplitudes are small, so that the angles the body makes with the swimming direction are close to zero. When angles become larger, more energy is lost into the wake than Eq. (8) predicts. Lighthill (1971) developed a large-amplitude version of the theory, which corrects for this effect and also predicts lateral forces, which are easier to compare to experimental measurements, as we will discuss later.

Both large- and small-amplitude elongated body theories suffer from an important problem. They make the assumption that the Reynolds number is effectively infinite, meaning that inertial forces completely dominate viscous forces. The Reynolds number, however, is a notoriously fuzzy concept. While the Reynolds number for the whole body may be very large and effectively infinite, the Reynolds numbers for the tip of the tail and the edges

of the fins are probably much smaller. In fact, you will almost always be able to find a structure small enough that its Reynolds number is too low to neglect viscosity. These viscous effects on small structures actually can be very important for forces on the overall body. First, they indicate that viscosity can never truly be completely neglected. Thus, resistive forces never become completely negligible. Second, and more importantly, viscous effects around sharp edges, like the trailing edge of an airfoil, can cause large changes in the flow around the body. For example, the lift force develops around an airfoil because of viscous effects around the sharp trailing edge (Faber, 1995). Wu (1971) developed a theory of fish swimming that incorporates an approximation of this effect.

Additionally, as we discussed previously, midline kinematics do not account for important differences in body shape. The virtual mass $m_V$ at the tail accounts for the caudal fin size, but trailing edges of dorsal, anal, pectoral, and pelvic fins, all of which are independently activated, are not represented in the theory. Weihs (1972) accounted for other fins in his model of rapid turns, but three-dimensional computational approaches (e.g., Zhu *et al.*, 2002) show more promise for modeling the diversity of swimming behaviors. Nonetheless, elongated body theory has been used regularly in fish swimming studies, both directly to make predictions of force, and indirectly to inform analyses of parameters such as efficiency (e.g., Weihs, 1972; Webb, 1975; Hess and Videler, 1984; Videler and Hess, 1984; Daniel and Webb, 1987; Müller *et al.*, 2002; Tytell, 2004a; Tytell and Lauder, 2004).

## IV. EXPERIMENTAL HYDRODYNAMICS OF UNDULATORY PROPULSION

Within the past 10 years, the ready availability of two new technologies has revolutionized our ability to study fluid flows generated by swimming fishes. Rather than use the theories described earlier to make hydrodynamic predictions based on kinematics, the combination of high-speed video and DPIV has allowed biologists to measure fluid flow directly. First, the new generation of high-speed video systems with resolution of at least 1024 by 1024 pixels, which can operate (at this resolution) at rates above 500 frames per second (fps), permits a whole new level of detail and resolution for imaging swimming fishes. Data obtained from such systems, particularly when cameras are synchronized for two or more simultaneous views of the swimming fish, permit highly accurate quantification of body and fin movements.

The true utility of such systems becomes evident when they are used with high-power continuous-wave lasers for DPIV, an engineering technique to quantify fluid flow by imaging small reflective particles in the flow (Willert and Gharib, 1991; Raffel *et al.*, 1998). Many engineering DPIV studies use pulsed lasers, which typically operate with a maximal temporal resolution of 15 Hz, and often much less, which is sufficient when steady flows are being studied but insufficient to understand the dynamic unsteady character of flows generated by swimming fishes. In contrast, recent biological DPIV work with high-speed video in combination with continuous lasers allows images of fluid flow patterns to be obtained at the full framing rate of the video (500 fps or greater), and can thus provide a detailed picture of flow separation and vortex formation by fins.

The experimental approach used to understand water flow during undulatory locomotion by freely swimming fishes is illustrated in Figure 11.5 (Anderson *et al.*, 2000; Drucker and Lauder, 2001a; Lauder and Drucker, 2002; Lauder and Drucker, 2004; Tytell and Lauder, 2004; Wilga and Lauder, 2004). Fishes swim in a recirculating flow tank and are induced to maintain station with their body or fins projecting into the laser light sheet, generated by a continuous argon ion laser and a series of focusing lenses. Small (12 $\mu$m mean diameter) near-neutrally buoyant reflective particles are mixed into the flow to provide reflections from the laser light sheet, which are recorded by a high-speed video camera. Images of fish position in the flow and relative to the light sheet are recorded by one or more additional synchronized video cameras. By reorienting laser optical components, it is possible to produce light sheets in different orthogonal orientations (Figure 11.5B and C) and hence obtain, in separate experiments, a three-dimensional impression of flow patterns. Images obtained from these high-speed videos (Figure 11.5D) are analyzed using standard DPIV cross-correlation techniques (Willert and Gharib, 1991; Raffel *et al.*, 1998) to yield a matrix of velocity vectors that estimate flow in the light sheet (Figure 11.5E).

Standard DPIV using a single video camera orthogonal to the light sheet produces only the two velocity components in the plane illuminated by the laser. It is also possible to use two cameras, offset by a known angle, to record stereo images and hence reconstruct the three components ($x$, $y$, and $z$) of flow velocity in a plane (e.g., Willert, 1997; Veerman and Den Boer, 2000; Westerweel and Oord, 2000). Stereo-DPIV data obtained for steady undulatory locomotion in trout (*Oncorhynchus*) were presented by Nauen and Lauder (2002b), who provided a simple three-dimensional analysis of the wake and calculated locomotor efficiency (see also Sakakibara *et al.*, 2004).

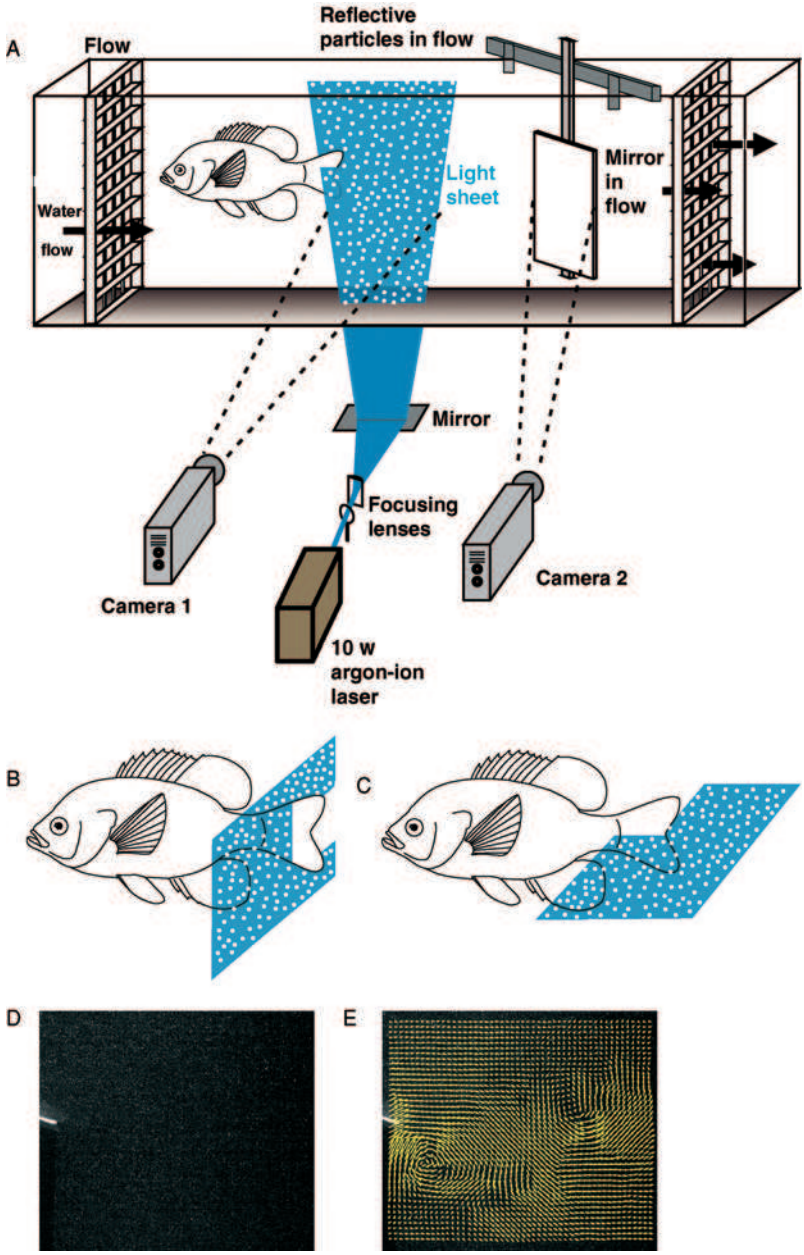
A
Flow
Reflective particles in flow
Water flow
Light sheet
Mirror in flow
Mirror
Focusing lenses
Camera 1
Camera 2
10 w argon-ion laser
B
C
D
E

These velocity vectors can then be used to estimate forces by analyzing the vorticity, a measure of the local angular velocity of a fluid element (Faber, 1995). Specifically, the vortex structure in the wake of a fish indicates the magnitude, angle, and, to some extent, timing of the forces the fish applied to the fluid. One can estimate force on the basis of this structure in two ways, both of which actually produce estimates of impulse, $I$, the average force multiplied by the time over which it was applied. By dividing the impulse by an appropriate time interval (typically half the tail-beat period), one can estimate average force. In the first, most commonly used method, researchers assume that counter-rotating vortices in the wake are connected above and below the plane to form a small-core vortex ring. By using multiple planes to measure the geometry of the ring, impulse can be estimated as

$$I = \rho A \Gamma, \tag{12}$$

where $\rho$ is water density, $A$ is the area circumscribed by the vortex ring, and $\Gamma$ is the circulation of the vortex cores (a measure of total vorticity in a region) (Batchelor, 1973). The second, and more rigorous, method applies the equation used to derive (12):

$$\mathbf{I} = \frac{1}{2}\rho \int \mathbf{x} \times \boldsymbol{\omega}\, dV, \tag{13}$$

where $\mathbf{I}$ is now a vector impulse, $\mathbf{x}$ is the position vector connecting a fluid element to the place the force was applied, and $\boldsymbol{\omega}$ is the vorticity vector (Batchelor, 1973). This method requires accurate estimation of vorticity, which is often difficult using DPIV, but potentially produces more accurate impulse estimates than Eq. (12) in wakes with complex vortex structure (Rosen *et al.*, 2004; Tytell, 2004a). Finally, Noca *et al.* (1999) derived a method to estimate true instantaneous force production, rather than average

**Fig. 11.5.** Experimental arrangement used for hydrodynamic analysis of water flow patterns over the body and in the wake of freely swimming fishes. Laser light sheet is shown in blue. (A) Fishes swim in a recirculating flow tank, maintaining station against oncoming flow. Optical components focus the laser beam into a thin (1–2 mm thick) light sheet, and fishes are positioned so that the body and/or tail intersect this light sheet. Small (12 $\mu$m mean diameter) reflective, nearly neutrally buoyant particles circulate with the flow. One high-speed video camera films reflections from these particles while a second camera monitors the position of the fish, either through a mirror or from above or below. The laser light sheet may be reoriented into two other orthogonal orientations (B, transverse plane; C, horizontal plane) in separate experiments to quantify flow in these planes. (D) Video images are analyzed using cross-correlation (Willert and Gharib, 1991) to yield matrices of velocity vectors (E, yellow arrows) estimating flow velocities through time.

forces from impulse estimates, but, to our knowledge, this approach has not been applied successfully in any studies of aquatic animal locomotion.

The experimental approach using flow tanks, high-speed video, and DPIV described previously has two significant advantages. First, the swimming speed and position of the fish can be accurately controlled by adjusting speed in the flow tank, and thus true steady swimming can be studied if care is taken during data acquisition. Controlled maneuvers can also be elicited from a known steady swimming posture (e.g., Wilga and Lauder, 1999; Drucker and Lauder, 2001b; Tytell, 2004b). Flow patterns can change considerably with speed or if fishes are accelerating (Drucker and Lauder, 2000; Tytell, 2004b). Second, use of multiple simultaneous cameras allows one or more cameras to record fish position in the laser light sheet (Figure 11.5A). It is difficult to overemphasize the importance of *both* controlling fish swimming speed *and* knowing where the fish is relative to the light sheet. Because of the complex three-dimensional body shape of most fishes, data obtained without knowing the position of the fins or body relative to the light sheet are extremely difficult to interpret. Other studies (Müller *et al.*, 1997, 2001) have applied DPIV to fish swimming in still water, which has the advantage that turbulence is lower, in principle, but recording steady behaviors is much more difficult.

## A. Axial Propulsion

Flow fields measured in the wake of swimming eels (*Anguilla*) show that oscillation of the body produces a wake with laterally oriented momentum jets and negligible downstream flow (momentum added opposite the direction of movement) (Figure 11.6; Müller *et al.*, 2001; Tytell and Lauder, 2004). Wake momentum is thus directed to the side and not in the streamwise direction along the axis of travel; each pulse of lateral momentum probably represents jet flow through the center of unlinked vortex rings. These lateral momentum jets are produced almost entirely by the final third of the body (Figure 11.7) and are not convected along the body via undulatory motion (Tytell and Lauder, 2004). Previously, structures termed "proto-vortices" had been observed along the body (Müller *et al.*, 2001). While these structures do exist (Figure 11.7), they do not contain much vorticity and are therefore not responsible for the vortex wake structure (Tytell and Lauder, 2004). As can be seen in Figure 11.7, there is very little vorticity upstream along the body. Instead, the posterior 15% of the body produces lateral jets of fluid, which results in strong (up to 90 $s^{-1}$) but unstable shear layers in the wake. The shear layer is visible between two regions of flow traveling in opposite directions, as between the first and second jets in Figure 11.6. The final wake forms through rollup of this shear

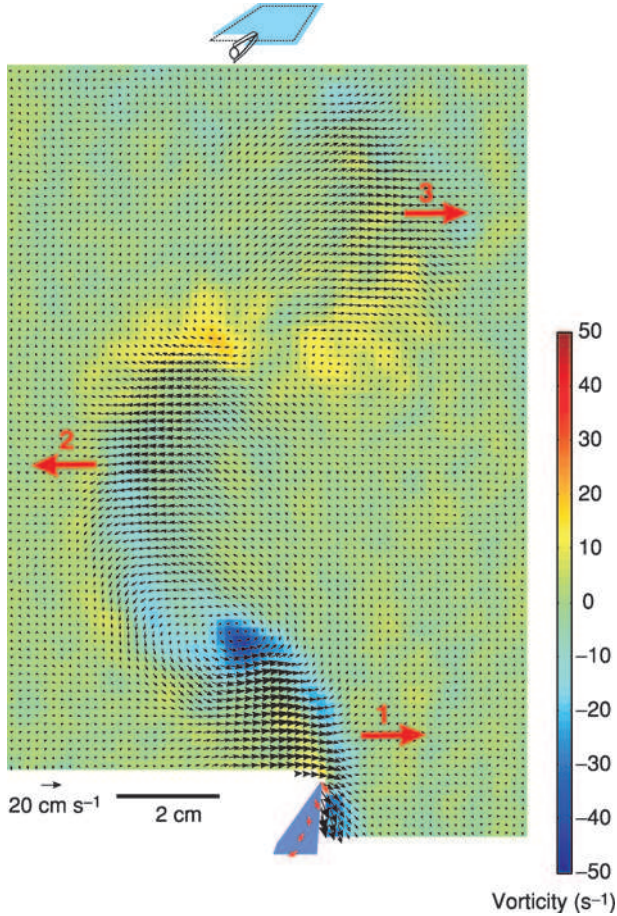


**Fig. 11.6.** Average flow field behind an eel (*Anguilla rostrata*) at 90% of the tail-beat cycle, recorded in the horizontal plane as shown schematically above and in Figure 11.5C. The vector field shown is a phase average of 14 tail beats. Vorticity is shown in color in the background, and velocity vectors, calculated from high-speed video images of the wake, are shown in black. The eel's tail is in blue at the bottom, with its motion indicated by small red arrows, scaled in the same way as the flow vectors. Freestream flow is from bottom to top and has been subtracted to show the vortex structure in the wake. Vector heads are retained on vectors shorter than 2.5 cm $s^{-1}$ to shown the direction of the flow; otherwise vector head size is scaled with velocity magnitude. Numbered large red arrows show the three regions of lateral momentum in the wake shed by the tail. (Modified from Tytell and Lauder, 2004.)

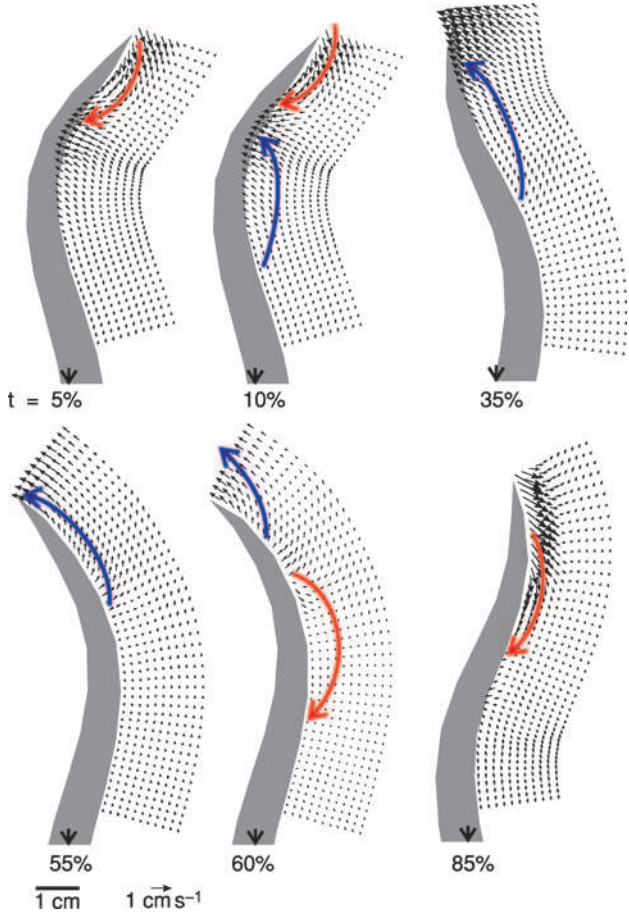


**Fig. 11.7.** Flow fields close to the body of a swimming eel (gray body outline). Velocity vectors are shown in black for six times during the tail-beat cycle. The lateral position of the eel's snout (off the view below) is shown as a black arrow. Velocities are phase averaged across 14 tail beats by interpolating the normal gridded coordinate system on to a system defined by the distance from the eel's body and the distance along the body from the head. Red and blue arrows indicate the major clockwise and counterclockwise flow directions, respectively, near the body. (Modified from Tytell and Lauder, 2004.)

layer (Figure 11.8), which separates into two or more vortices that are fully developed approximately one tail-beat cycle later. This vortex shedding pattern matches well the pattern of body kinematics (Figure 11.1) with relatively little oscillation of the front half of the body.

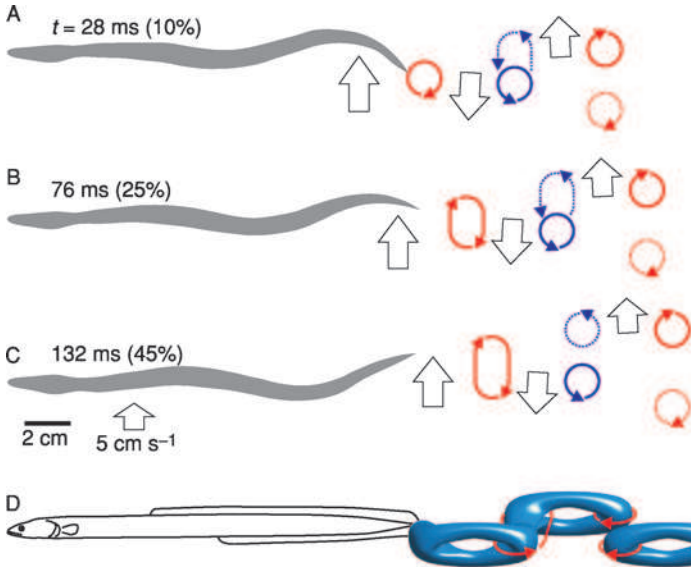


**Fig. 11.8.** (A–C) Schematic diagram of wake formation behind a steadily swimming eel, *Anguilla*. Vortices shed by the tail are shown at three different times in the locomotor cycle as red and blue arrows; primary vortices are solid, while secondary vortices formed by roll-up of the shear layer shed by the tail are shown as dotted lines. Lateral momentum jets to each side are indicated by block arrows. (Modified from Tytell and Lauder, 2004.) (D) Hypothesized three-dimensional flow, based on (A–C). Lateral vortex rings (shown in blue) are partially linked at the shear layer, but separate completely in the far wake.

As eels increase their swimming speed over a range from 0.5 to 2.0 $Ls^{-1}$, the fundamental character of the wake does not change (Tytell, 2004a). As long as swimming is steady, there are large lateral momentum jets and little streamwise momentum added to the wake.

In contrast to the wake structure of eels, the wake of fishes such as trout, mackerel, or sunfish shows considerable streamwise momentum (Lauder *et al.*, 2002, 2003; Nauen and Lauder, 2002a,b). Figure 11.9 shows a horizontal slice through the wake of a swimming trout, *Oncorhynchus*. Two distinct centers of vorticity are present in this mid-body wake section, as is a substantial central momentum jet with a strong downstream component. A vertical slice through the wake flow (see Figure 11.5A) of mackerel reveals distinct tip vortices and provides another view of the downstream component of the tail momentum jet (Figure 11.10A). Taken together, the horizontal and vertical wake slices suggest that mackerel, trout, and bluegill produce a linked vortex ring structure in their wakes (Figure 11.10B). Also, note that

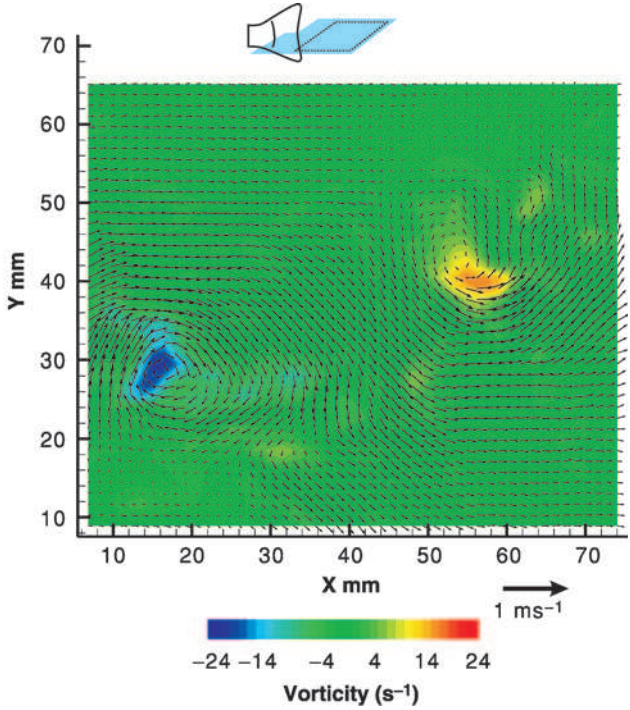


**Fig. 11.9.** "Subcarangiform" wake flow pattern in the horizontal plane from a freely swimming trout (*Oncorhynchus mykiss*) swimming steadily at 1.0 $Ls^{-1}$. Light sheet orientation is shown schematically above. Freestream flow is from left to right and has been subtracted to reveal two vortex centers produced by the caudal fin. These two vortex centers represent a planar section through a vortex ring with a high velocity central momentum jet directed downstream and laterally. (Modified from Lauder *et al.*, 2002.)

although downstream momentum is present in fishes as diverse as bluegill sunfish and mackerel, lateral forces are almost always at least equal to streamwise forces and are often as much as two to three times larger (Figure 11.10B) (Lauder and Drucker, 2002; Nauen and Lauder, 2002a).

While this wake structure is different from that of eels, the vorticity pattern in a horizontal section along the body of fishes with distinct tails is similar to that observed in eels (compare Figure 11.11 to Figure 11.7). In both cases, virtually all wake vorticity is developed along the posterior third of the body.

Anderson *et al.* (2000) performed a much more detailed analysis of flow close to the body than is shown in Figures 11.7 and 11.11. By examining the boundary layer, a region close to the body where fluid velocities change from the free stream flow velocity to the body velocity, they estimated skin friction

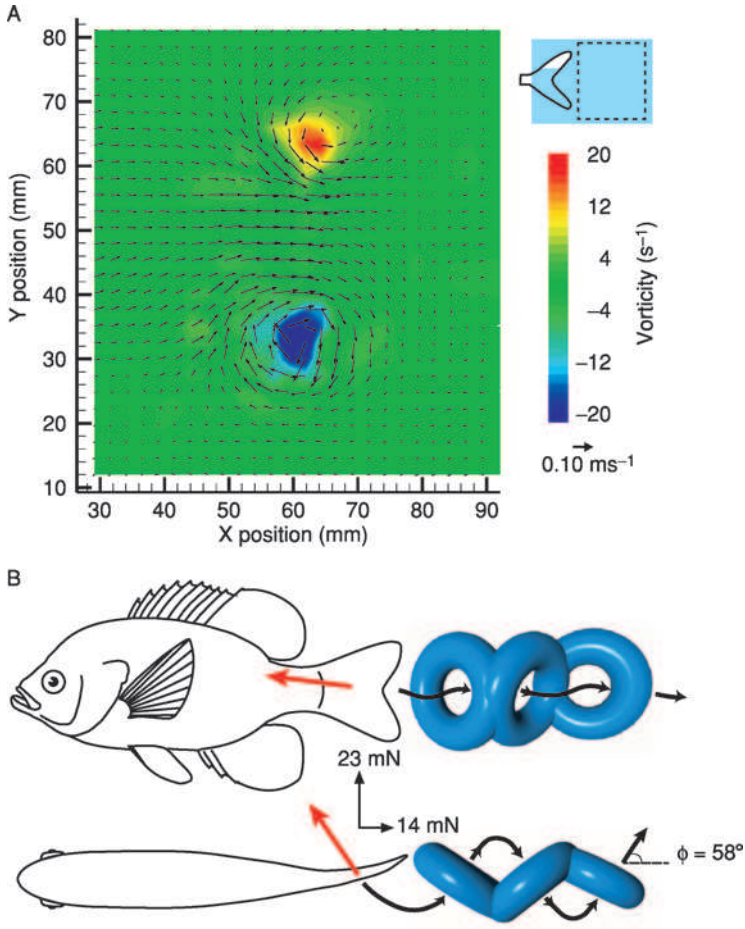


**Fig. 11.10.** (A) Flow field in the vertical plane in the wake of mackerel (*Scomber japonicus*) swimming steadily at 1.2 $Ls^{-1}$. Two centers of vorticity are clearly present that were shed by the dorsal and ventral tips of the tail, and the central momentum jet through the tail vortex ring is visible as accelerated flow between the vortex centers. Light sheet orientation is shown schematically above. (Modified from Nauen and Lauder, 2002a.) (B) Schematic model of vortex rings (shown in blue) in the wake of fishes with discrete caudal fins, showing both lateral and dorsal views. During steady locomotion at 1.5 $Ls^{-1}$ the tail sheds linked vortex rings with a central jet of high momentum flow, shown as thick black arrows weaving through the vortex ring centers. For bluegill sunfish (*Lepomis macrochirus*) swimming at this speed, the high-velocity jet flow makes an average angle of 58° with the axis of progression, and the tail generates a mean thrust force of 14 mN, with a mean side force of 23 mN. The reaction force on the tail is shown as a red arrow. (From Lauder and Drucker, 2002.)

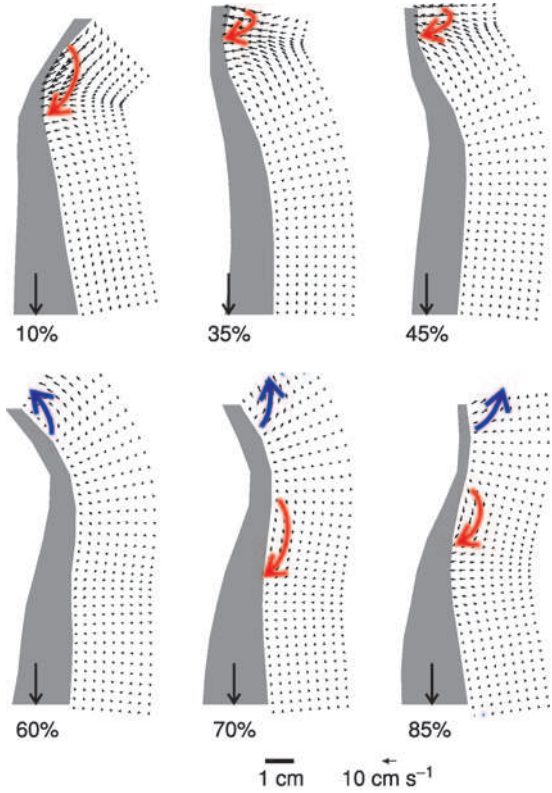


**Fig. 11.11.** Flow fields close to the body of a swimming bluegill sunfish (*Lepomis macrochirus*, gray body outline) swimming in a "subcarangiform" mode at 1.65 $Ls^{-1}$. Velocity vectors are shown in black for six times during the tail beat cycle. The lateral position of the sunfish's snout (off the view below) is shown as a large black arrow. Red and blue arrows indicate the major clockwise and counterclockwise flow directions, respectively, near the body.

drag on the bodies of freely swimming scup (*Stenotomus chrysops*) and smooth dogfish (*Mustelus canis*). The magnitude of the drag force on a swimming body has been long debated, with some suggesting that fishes can reduce their drag below that of a stretched straight body (Gray, 1936; Barrett *et al.*, 1999) and others suggesting it should be higher (Lighthill, 1971; Webb, 1975). The Anderson *et al.* (2000) boundary layer measurements clearly indicate that undulatory motion increases drag on both carangiform and anguilliform swimmers.

The differences between the wakes from these two types of swimmers may result less from differences in their midline kinematics (Figure 11.1),

and more from differences in the body shapes between eels and other fishes, particularly differences in their tails (see Figure 11.2). Midline kinematics between these fishes are not identical, but the differences are small, whereas their body shapes are very different. The wake differences indicate an important physical difference, as well. When fishes swim steadily, the total drag force must balance thrust over a tail-beat cycle, leading Schultz and Webb (2002) to suggest that there should be no thrust signature in the wake. Indeed, this is what is observed for eel locomotion (Figure 11.6) but not for data from fish such as trout, bluegill, and mackerel that have discrete caudal fin propulsors (Figures 11.9 and 11.10). Tytell and Lauder (2004) and Fish and Lauder (2005) suggested that the tails of such fishes function as a discrete propeller, separate anatomically and functionally from the major areas incurring drag during undulatory locomotion. In a boat with an external motor, the hull of the boat incurs the majority of drag, while the propeller is a separate thrust-generating structure. Sections of a boat wake behind a propeller show a clear thrust signature, just as the wake behind fishes with discrete caudal fins demonstrates thrust. By analogy, the caudal fin of fishes functions as a propeller, with its own intrinsic musculature powering movement. It is not surprising, then, that a clear thrust signature is evident in both experimental wake flow visualizations and in three-dimensional computational models that include a distinct tail propulsor (e.g., Zhu *et al.*, 2002).

## B. Function of the Tail

Many fishes have exquisite control over the motion of their tail, allowing them to vary the relative magnitudes of thrust, lateral forces, and lift forces. Even fishes with externally symmetrical (homocercal) tail structures can control the shape and motion of the dorsal and ventral lobes, which usually results in asymmetrical motion and influences the direction of wake flow (Lauder, 1989, 2000; Lauder *et al.*, 2003). Figure 11.12 shows the shape of the caudal fin during one fin beat by a steadily swimming bluegill sunfish: the dorsal lobe of the tail may undergo greater lateral excursion than the ventral lobe, and the tail expands and contracts vertically during the tail beat. Intrinsic tail muscles actively produce these changes in fin conformation (Lauder, 1982, 1989).

Wilga and Lauder's (2002, 2004) studies on sharks indicate some possible hydrodynamic effects from this asymmetrical motion. They performed DPIV in the wake of sharks, which also move their tails asymmetrically. In this case, the inclined trailing edge of the morphologically asymmetrical (heterocercal) caudal fin results in a ring-within-a-ring vortex structure in the wake (compare Figure 11.13 to Figure 11.10B). It is currently unknown

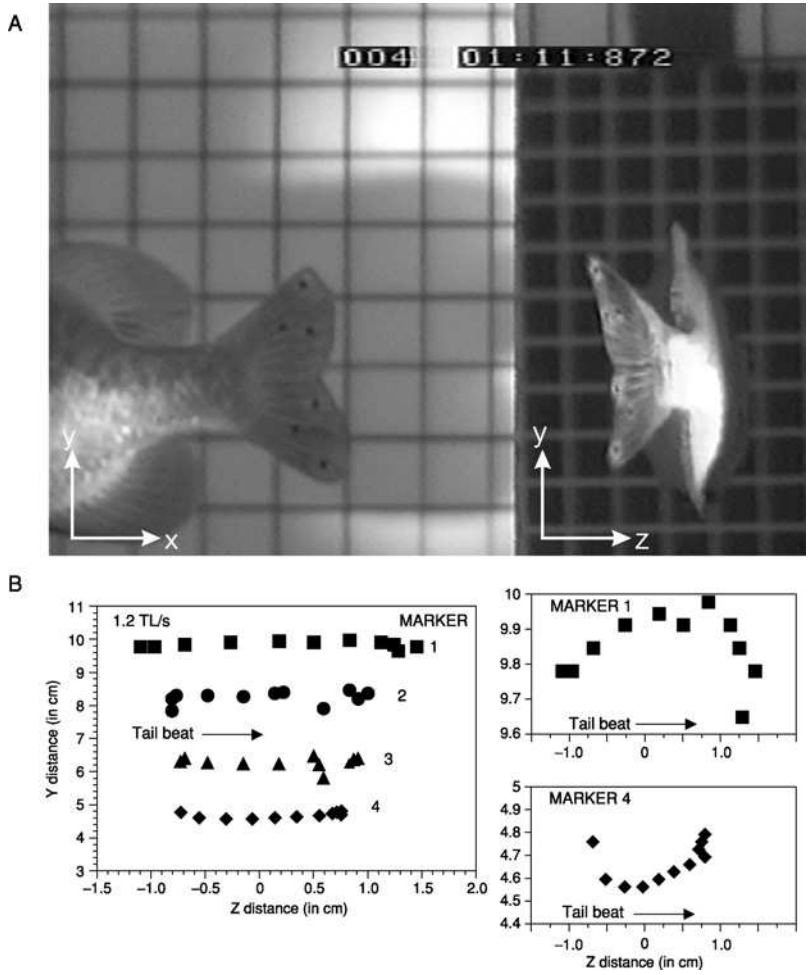


**Fig. 11.12.** Tail movement in fishes with a homocercal (externally symmetrical) tail need not be symmetrical. (A) Two synchronized video frames showing tail position in bluegill sunfish (*Lepomis macrochirus*) during steady rectilinear locomotion at 1.5 $Ls^{-1}$. The left panel shows the lateral (*xy*) view, while the right panel shows a posterior (*yz*) view through a mirror located in the flow, as illustrated in Figure 11.5. The tail trailing edge has been marked on each side with four small black markers to facilitate digitizing trailing edge angles and excursions. (B) Plot of *yz* excursions of four tail markers. Tail motion is from left to right. Note that the dorsal tail lobe can undergo considerably greater excursions than the ventral lobe. The two panels to the right show expanded views of dorsal (marker 1) and ventral (marker 4) excursions to demonstrate how the fish expands its tail during the beat. (Modified from Lauder, 2000.)

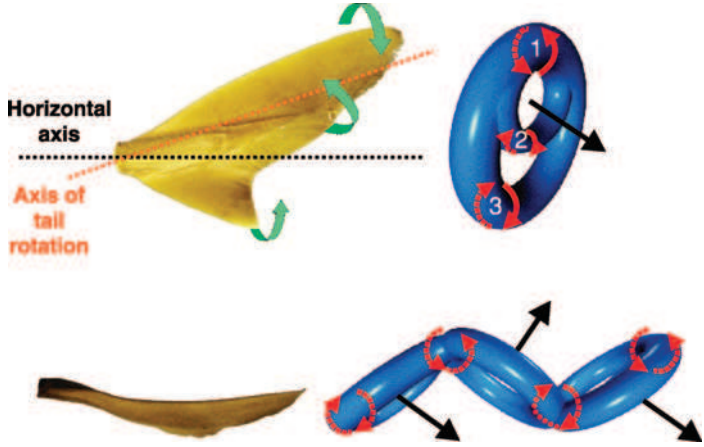


**Fig. 11.13.** Schematic ring-within-a-ring vortex ring structure in lateral and dorsal view shed by the heterocercal (externally asymmetrical) tail of a swimming spiny dogfish shark (*Squalus acanthias*). Three centers of vorticity are seen in the wake (red curved arrows, numbered 1 to 3 from dorsal to ventral). The central momentum jet through the upper ring is shown as black arrows. Curved green arrows show fluid separating around the tail tips and inclined trailing edge. (Modified from Wilga and Lauder, 2004.)

whether the asymmetric motion described above in fishes such as sunfish that have homocercal tails affects the flow in a similar way; the conformational changes these fishes use may also introduce additional hydrodynamic complexity.

Thus, the tail should not be viewed as a simple extension of the body, a view encouraged by kinematic and hydrodynamic models of fish propulsion based on horizontal mid-body sections (Figures 11.1, 11.2, and 11.4). Rather, the fish tail functions as a independent propulsive surface with distinct three-dimensional anatomy, shedding vortices and used to adjust overall body trim (Liao and Lauder, 2000; Wilga and Lauder, 2002).

Finally, it should be emphasized that flow passing over the tail is affected by the body upstream of it. In mackerel, for example, flow over the body converges toward the tail (Figure 11.14A and B), producing a complex flow around the caudal peduncle. Quantification of particle motion in this region suggests that overall flow results from a combination of two patterns: converging flow along the body, and flow wrapping around the peduncle as it moves from side to side (Figure 11.14C and D) (Nauen and Lauder, 2001). The tail thus does not see freestream flow, but rather encounters flow altered by the body and caudal peduncle. Further alteration of incident tail flow occurs by the dorsal and anal fins, as is discussed in the next section.

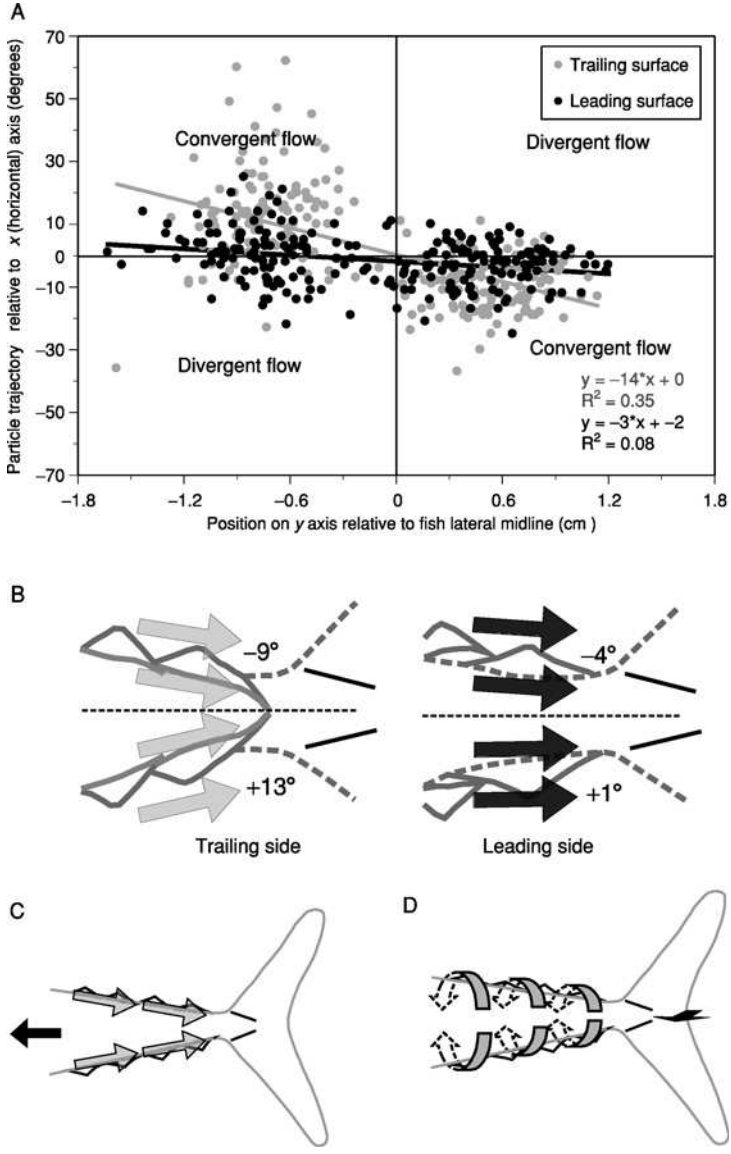


**Fig. 11.14.** Flow patterns in the region of the caudal peduncle and leading edge of the tail in mackerel (*Scomber japonicus*) swimming steadily at 1.2 $Ls^{-1}$, measured by manually tracking particle motion. Each symbol represents the position of an individual particle in the flow field. (A) Particle trajectories relative to the horizontal for flow on the leading peduncular surface (black dots) and trailing surface (gray dots). Linear regressions for each flow type show negative slopes, indicating that flow is converging toward the midline of the tail. (B) Schematic summary

## C. Dorsal and Anal Fin Function

The dorsal and anal fins of fishes are important fluid control structures with their own intrinsic musculature (Gosline, 1971; Geerlink and Videler, 1974; Winterbottom, 1974; Jayne *et al.*, 1996), ability to exert force on the fluid environment (Arreola and Westneat, 1997; Hove *et al.*, 2001; Standen and Lauder, 2005), and discrete sharp trailing edges at which flow separation may occur (Drucker and Lauder, 2001a; Lauder and Drucker, 2004). However, these fins have not received much attention in the hydrodynamic literature on undulatory propulsion, although some computational models do include passive median fins (Wolfgang *et al.*, 1999; Zhu *et al.*, 2002). Webb (1978) and Webb and Keyes (1981) also discussed vortex sheets that could be shed from median fin trailing edges. In part this lack of attention may be due to the difficulty of studying fin function experimentally and to the primary focus of many studies on undulation of the body midline itself.

Key evidence that dorsal and anal fins play an important role in the overall force balance during locomotion is provided by DPIV analyses of their wakes (Figure 11.15). By recording dorsal fin wake flow patterns in the horizontal plane (Figure 11.16A, planes 1, 2), it is clear that streamwise momentum is added to the wake and that substantial side forces are produced by oscillating dorsal fins (Lauder and Drucker, 2004). In bluegill sunfish, the soft dorsal fin contributes nearly 12% of overall locomotor thrust force at a swimming speed of 1.1 $Ls^{-1}$, and dorsal fin lateral force is nearly twice thrust force (Drucker and Lauder, 2001a). In trout, lateral forces are even higher relative to thrust force (greater than three times), because the dorsal fin wake oscillates laterally, adding little downstream momentum (Figure 11.15B). Dorsal fins in bluegill and trout thus actively generate considerable side force, which may contribute to body stability during locomotion.

The dorsal and ventral lobes of the caudal fin pass through the wake shed by dorsal and anal fins. The hydrodynamic environment experienced by the tail is thus substantially different than the freestream flow that might be assumed in the absence of other median fins. In bluegill, dorsal fin wake vortices encounter the tail and accelerate flow over the tail surface (note the velocity vectors around the caudal fin in Figure 11.15A) (Drucker and

---

of mean particle tracks in (A) (large grey and black arrows representing trailing and leading flows) giving the mean angle of convergent flow on both sides of the tail. (C and D) Schematic hypothesis of the two peduncular flow patterns that combine to produce the pattern seen in panels (A) and (B): observed flow is the result of convergence along the body surface as it slopes toward the tail midline (C), and divergence results from side-to-side motion in which flow encircles the peduncle (D). (Modified from Nauen and Lauder, 2001.)

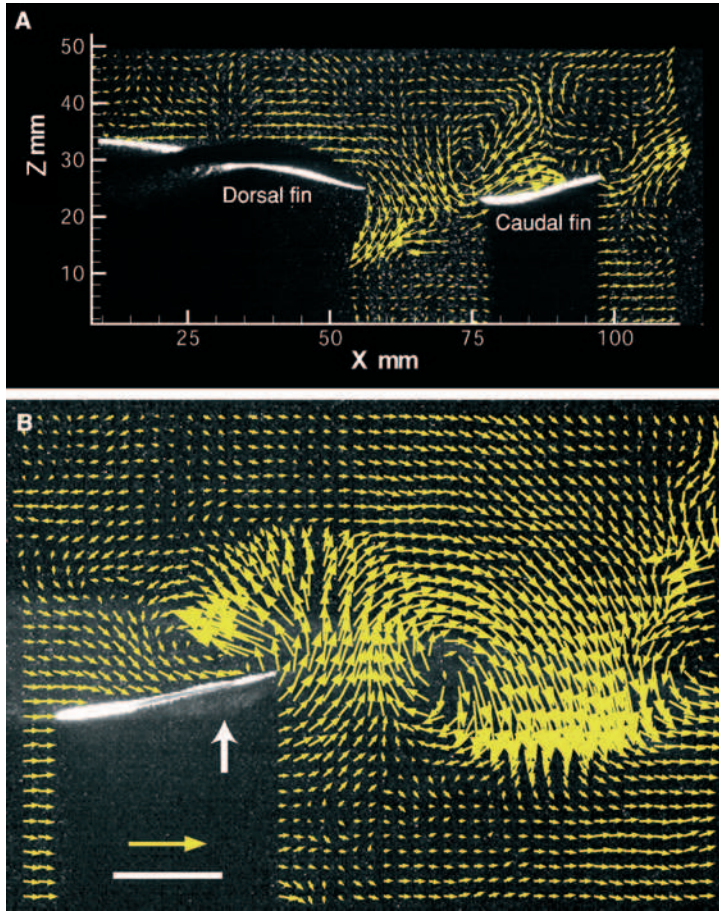


**Fig. 11.15.** The dorsal fin of bony fishes is an active component of locomotor design and sheds a discrete wake that alters incident flow at the tail. Both panels show flow as viewed from above (*xz* plane). (A) Dorsal fin wake in bluegill sunfish, *Lepomis macrochirus*. The dorsal fin has accelerated flow in the gap between the dorsal fin and tail, and has shed a vortex located just above the tail in this image. (B) The dorsal fin wake in rainbow trout (*Oncorhynchus mykiss*) sheds a linear array of vortex centers with strong lateral jets to each side. The tail passes through these jets and through the centers of the dorsal fin vortices. White arrow pointing up in panel (B) shows the direction of trout dorsal fin motion. Scales: arrow = 10 cm/s; bar = 1 cm. Mean freestream flow has been subtracted from each image. (Modified from Drucker and Lauder, 2001a; Lauder and Drucker, 2004.)

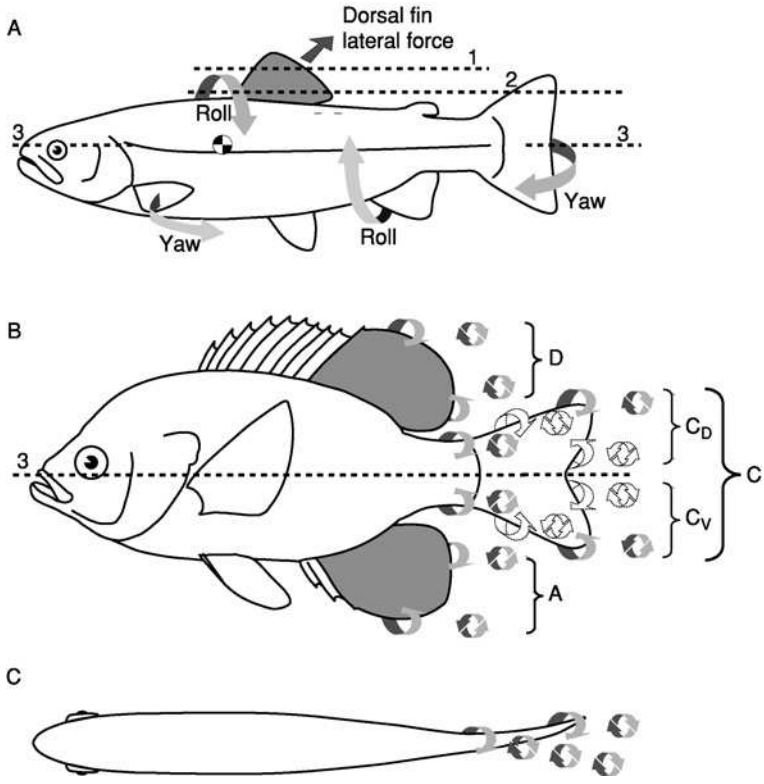


**Fig. 11.16.** (A) Schematic summary of the overall force balance on freely swimming fishes based on recent particle image velocimetry data. The dorsal fin generates lateral forces (see Figure 11.15) with accompanying yaw and roll torques around the center of mass. These torques must be countered by the action of the caudal, pectoral, and anal fins. The three numbered lines show alternative horizontal slices through the fish at which the wake shed by the body and fins has been analyzed: 1, wake of the dorsal fin alone; 2, wake of the dorsal fin and tail; 3, midline flow of the body and tail (Drucker and Lauder, 2001a; Lauder *et al.*, 2002; Lauder and Drucker, 2004; Tytell, 2004a; Tytell and Lauder, 2004). (B) Hypothesis of streamwise vortical separation from the caudal, dorsal, and anal fins and the caudal peduncle in lateral view. Vortices are shed from the dorsal (D), anal (A), and caudal (C) fins. The dorsal and ventral lobes of the caudal fin may shed discrete vortices also ($C_D$ and $C_V$). (C) Horizontal section through the middle of the fish at the level of line 3 in (B). Because of undulatory motion, flow rolling up around the caudal peduncle may not be destroyed by the tail, but may instead result in discrete vortices in the wake. Only the upper vortices shed by the caudal peduncle and tail are shown. [Panel (A) modified from Lauder and Drucker (2004).]

Lauder, 2001a). This suggests that dorsal fin vortices might increase tail thrust if caudal fin surface pressures are reduced below what they would be without the dorsal fin. Computational fluid dynamic modeling of dorsal-caudal fin wake interactions corroborates this view, and indicates that vorticity shed from the dorsal fin promotes more rapid growth of the leading edge vortex on the caudal fin, enhancing thrust (Mittal, 2004).

Some fishes such as tuna swim routinely with the dorsal fin retracted (except during maneuvering). In such cases, the tail encounters flow altered only by the body, and roll stability must be achieved by adjusting the position of pectoral fins, which are held in a partially extended position during most routine locomotion (Magnuson, 1978).

### D. Overall Force Balance and Three-Dimensional Flow

The large lateral momentum produced by the dorsal fin in ray-finned fishes has important consequences for the overall force balance during locomotion (Figure 11.16A). This lateral force is generated above and posterior to the center of mass and must thus generate both roll and yaw torques. In order for fishes to swim steadily without roll and yaw, other fins must compensate. To counter roll torques induced by the dorsal fin, the anal fin could generate an opposing torque by generating lateral momentum to the same side as the dorsal fin (Figure 11.16A). In addition, the tail and pectoral fins may act in concert to correct any yaw torques.

Overall, the picture that emerges from experimental studies of median fin function is that a complex force balance exists among all fins and the body and tail, even during steady rectilinear locomotion. Both median and paired fins act in concert with the tail to stabilize the body. In light of these experimental data, the classical categorization of locomotor modes as BCF (body-caudal fin) as distinct from MPF (median-paired fin) seems extremely simplistic, if not directly misleading, as median fins clearly are hydrodynamically active during body and caudal fin locomotion, and may in fact play a crucial role in body stability.

Understanding the overall force balance on swimming fishes requires data on buoyancy, body shape, body position, and the direction of forces produced by the fins and body. Despite these complications, progress has been made by quantifying body angles and flow over the body, and by experimental investigation of individual fin forces. Many fishes swim with a positive angle of attack to the body (He and Wardle, 1986; Webb, 1993a; Wilga and Lauder, 1999; Liao and Lauder, 2000; Wilga and Lauder, 2000; Nauen and Lauder, 2002a; Svendsen *et al.*, 2005). This appears to be critical to the overall force balance because body angle changes as swimming speed increases, altering the lift force due to flow over the body.

An additional complication for understanding the overall force balance on swimming fishes is the three-dimensional nature of flow around the body and tail. Figure 11.16B illustrates one possible pattern of flow separation from the trailing edge of the dorsal, anal, and caudal fins, as well as the caudal peduncle in ray-finned fishes. The homocercal tail itself could generate additional small vortices due to rollup at the inclined edges near the midline, by analogy with flow around the heterocercal shark tail (Figure 11.13) (Wilga and Lauder, 2004), although these have yet to be seen experimentally. As seen in a posterior (*yz*) view, then, the vortex wake could consist of as many as 10 vortex filaments: two pairs shed by the tail, one pair by the caudal peduncle due to flow separation at the upper and lower edges, and one pair each by the dorsal and anal fins. How these link up to form discrete vortex rings (Figure 11.10B) is not currently known. Even if the tail moves so that only a single large vortex ring is shed by the caudal fin, additional vortex rings from the dorsal and anal fin may still exist in the wake, producing complex interactions among them. These speculations remain to be examined experimentally, because the structure of streamwise vorticity near the tail and caudal peduncle has not yet been observed. But the importance of three-dimensional effects for understanding fish undulatory hydrodynamics is clear.

### E. Undulatory Locomotion in Turbulence

In nature, fishes rarely swim in controlled flows like those produced in laboratory flow tanks. Indeed, one might argue that the vast majority of the locomotor time budget for fishes is spent in turbulent flows. From rapidly flowing streams to strong ocean currents passing over an uneven benthic habitat, most fish habitat is turbulent. While it is certainly understandable that the vast majority of research has used controlled microturbulent flows in laboratory flow tanks to study locomotion, fishes exhibit a wide array of locomotor behaviors such as drafting or entraining on obstacles in turbulent flows (Sutterlin and Waddy, 1975; Gerstner and Webb, 1998; McLaughlin and Noakes, 1998; Webb, 1998). In addition, the use of much larger "natural" flow environments to study fish locomotion (Castro-Santos, 2004, 2005; Haro *et al.*, 2004) reveals new strategies and levels of performance that are not accessible in laboratory settings (Chapter 12).

One example of an unusual locomotor behavior in larger-scale turbulent flows has been termed the "Kármán gait" by Liao *et al.* (2003a,b). By using a D-section cylinder to generate a regular array of alternating vortices in a Kármán vortex street (Figure 11.17), Liao *et al.* observed that a variety of fish species radically alter their locomotor kinematics when swimming in vortical flows. During locomotion in freestream microturbulent flows, fishes

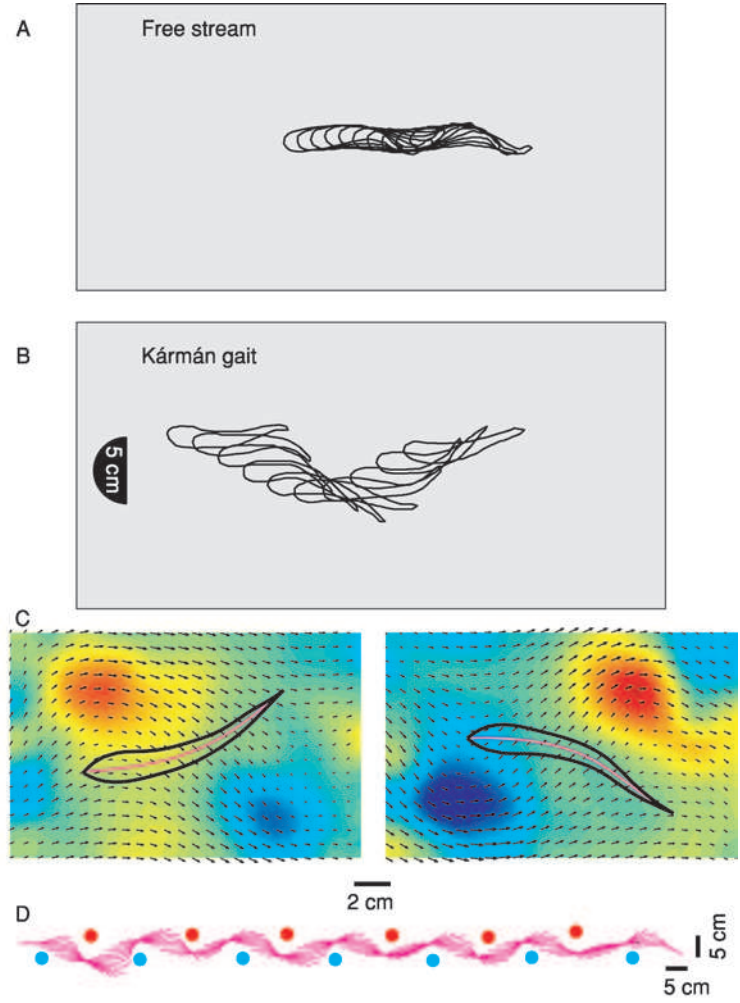


**Fig. 11.17.** The Kármán gait. (A and B) Trout (*Oncorhynchus mykiss*) swimming in standard freestream microturbulent flow (A) exhibit small lateral oscillations of their center of mass compared to locomotion in a Kármán vortex street behind a D-section cylinder (B). The presence of Kármán vortices radically alters locomotor kinematics in fishes. Fishes in the Kármán street swam three to four body lengths downstream from the D-section cylinder (5 cm wide), well downstream of the suction region behind the cylinder. (C) Quantification of trout body position relative to vortex centers. The trout body outline is shown in black, the midline as a red line, and background flow vorticity in color with superimposed black velocity vectors. (D) During locomotion in a vortex street, trout weave in between vortex centers: trout midlines are shown as red lines during locomotion from right to left, and centers of positive and negative vorticity are indicated by red and blue dots. Flow is from left to right in all plots. (Modified from Liao *et al.*, 2003a,b.)

exhibited the usual pattern of body undulation with only small oscillations of the center of mass (Figure 11.17A; also compare to Figures 11.1 and 11.2). However, in a Kármán vortex street, fishes substantially altered the pattern of body undulation (Figure 11.17B) and displayed very large center of mass oscillations and large-amplitude variations in lateral excursion along the body. In addition, by using DPIV to record simultaneous flow and kinematic patterns during the Kármán gait, Liao *et al.* (2003a) showed that fishes weave in between oncoming vortices (Figure 11.17C and D). The pattern of body bending appears to be primarily passive; both red and white myotomal musculature are largely inactive during the Kármán gait (Liao, 2004). Fishes may use pectoral fins or anterior red myotomal musculature to adjust the body angle of attack to oncoming vortices, but otherwise de-recruit middle and posterior body musculature.

## F. Acceleration and Maneuvering

Very few studies have quantified either linear or angular acceleration in fishes as part of the normal undulatory locomotor repertoire (see Webb, 1991). Of course, high-speed unsteady C-start movements with high accelerations and rapid turns have been studied frequently (see Chapter 9), but we know little about routine (low-speed) linear acceleration and turning by fishes and their hydrodynamic causes. Drucker and Lauder (2001b) analyzed the wake of the dorsal fin during controlled yawing maneuvers, and studies by Wolfgang *et al.* (1999), Anderson (1996), and Anderson and Chhabra (2002), and Müller *et al.* (2002) provided some data on the vortices formed by turning fish. But these data lack accompanying detailed kinematics to provide a link between the pattern of body undulation and wake hydrodynamics.

Tytell (2004b) studied controlled linear accelerations in eels (*Anguilla*) under conditions that allowed quantification of both kinematics and the hydrodynamic wake from the same individual locomotor sequences. Eels accelerated or decelerated at rates ranging from 1.3 to $-1.4$ $L\text{s}^{-2}$, starting from steady undulatory locomotion at speeds that varied from 0.6 to 1.9 $L\text{s}^{-1}$. These experiments showed that eels primarily varied tail tip velocity to power acceleration, and that acceleration was accompanied by the addition of significant streamwise momentum to the wake (Tytell, 2004b). The wake of an accelerating eel thus takes on the appearance of the standard undulatory wake in fishes with discrete caudal fins and a downstream momentum jet (e.g., Figures 11.9 and 11.10). Changes in wake structure during linear acceleration in fishes with distinct median and caudal fins have yet to be studied.

## V. INTEGRATING THEORY AND EXPERIMENTAL DATA

Comparison of elongated body theory to experimental data (and validation of the model) has mostly used energetic data on swimming efficiency, as this was the only available body of data that permits comparison to theory (Webb, 1975, 1978). Webb (1978, p. 215) noted that "Ideally, validation would be based on observations of flow about swimming fish ..." and indicated that such observations were problematic at that time. However, the ability in recent years to directly quantify water flow patterns over the body and fins of fishes using DPIV provides a new opportunity to compare experimental hydrodynamic data on fish locomotion to predictions of theoretical models (such as that of Lighthill, 1960), computational models (Carling *et al.*, 1998; e.g., Fauci and Peskin, 1988; Wolfgang *et al.*, 1999; Liu, 2002; Zhu *et al.*, 2002; Cortez *et al.*, 2004; Mittal, 2004), and the results of experiments by fluid engineers on heaving and pitching foils (Triantafyllou *et al.*, 1993; Gopalkrishnan *et al.*, 1994; Anderson *et al.*, 1998; Hover *et al.*, 1998, 2004; Read *et al.*, 2003; Triantafyllou *et al.*, 2004). Both avenues promise to provide considerable insight into the mechanistic bases of force generation during undulatory locomotion, but are still relatively unexplored.

Tytell and Lauder (2004) and Tytell (2004a) compared several parameters measured from DPIV analyses of the wake of swimming eels to predictions of wake impulse derived from Lighthill's elongated body theory (EBT). They found good agreement in estimates of power, but poor agreement in force and impulse estimates. Mean lateral wake power calculated from DPIV was not statistically different from the value calculated from EBT. The overall shape of the wake power profile as it varies over time is also similar for both DPIV and EBT, although DPIV methods generate higher peak power estimates than EBT. However, EBT generally underestimates the wake forces as calculated from DPIV, by as much as 50%.

It is somewhat surprising that agreement was observed in power but not in force. One might expect that either both or neither would agree. However, fluid dynamic effects not included in EBT may affect the wake power without changing the force output substantially (Lighthill, 1971; Webb, 1975), and vice versa. Additionally, discrepancies between DPIV and EBT may come from the assumptions required in DPIV force and power estimates about the three-dimensional structure of the wake. DPIV measures only a single slice of the wake and thus requires assumptions about the flow outside of this slice. Errors in three-dimensional reconstruction may hence

under- or over-estimate total wake vorticity. Finally, measuring wake power accurately with DPIV through an entire control volume is difficult.

## VI. PROSPECTUS

Over the past 10 years, the development of new video and laser imaging technologies has permitted advances in the study of undulatory hydrodynamics in fishes that were not anticipated at the time the previous major reviews of fish propulsion were written (Lindsey, 1978; Magnuson, 1978; Webb, 1978; Blake, 1983; Webb and Weihs, 1983; Videler, 1993). Detailed analyses of fin and body wake flow patterns are now possible, and recent developments allow measurements of all three velocity components (Nauen and Lauder, 2002b), quantification of undulatory profiles under controlled swimming conditions (Dewar and Graham, 1994; Jayne and Lauder, 1995; Gillis, 1998; Donley and Dickson, 2000; Donley and Shadwick, 2003), and correlations between kinematic and hydrodynamic patterns (Tytell, 2004b). These advances have suggested the need for reevaluating previous classification schemes for fish swimming, and have provided a wealth of new information on how the body and fins interact with the fluid environment.

However, there is still much to learn. We see the following five areas as key directions for future progress. First, to date there has been only limited interaction between researchers developing computational fluid dynamic (CFD) models of undulatory propulsion (e.g., Fauci and Peskin, 1988; Williams *et al.*, 1995; Liu *et al.*, 1996; Carling *et al.*, 1998; Liu, 2002; Cortez *et al.*, 2004; Mittal, 2004) and workers conducting the experimental hydrodynamic studies described here. Additional boundary layer measurements, like those of Anderson *et al.* (2000), are especially key, as they allow direct comparisons of theoretical and empirical estimates of drag forces, which are not measurable through wake flow visualization (Tytell and Lauder, 2004). Future experimental work could focus on testing specific predictions of computational models (as was done for eels; Tytell and Lauder, 2004), on validating those models, and on collaborative studies to investigate new phenomena such as dorsal-caudal fin wake interactions.

Second, we have very little experimental data on three-dimensional flow patterns over the body and fins in swimming fishes. Such data are critical for understanding the vortical structure of the wake, for understanding how fins interact with each other hydrodynamically, and for testing assumptions of theoretical models of fish propulsion. In addition, quantifying three-dimensional flow patterns is necessary to understand the hydrodynamic significance of differences among fish species in body shape, and, specifically,

to determine why eel-shaped fish bodies produce a wake different from fishes with discrete caudal fins.

Third, there are currently few data on maneuvering and locomotion in turbulent flows. Both of these locomotor modes are in need of substantial experimental study if we are to understand more completely the locomotor repertoire of fishes.

Fourth, the function of fins and their hydrodynamic interactions with movement of the body is still a largely unexplored area. A hallmark of fish functional design is the use of multiple control surfaces projecting from the body (Lauder and Drucker, 2004), yet we have only modest data on dorsal fin function, a smattering of data on the anal fin, and effectively no data on the function of pelvic fins.

Finally, studies of external hydrodynamics need to be better connected to internal body mechanics, muscle activity and, ultimately, the neural circuitry that controls locomotion. The flow patterns discussed in this chapter develop due to a complex balance between the forces they apply to a fish's body and the forces a fish's muscles apply back to the fluid. The dynamics of this coupling have been preliminarily approached by Cortez *et al.* (2004), but substantially more research must be done to understand it better. Ultimately, these forces are controlled and modulated by the nervous system (Grillner, 2003), which itself responds to feedback from the same hydrodynamic forces. Integrating experimental and computational studies of hydrodynamic flow patterns with research on the mechanics of the body and the neural control of locomotion (Williams *et al.*, 1995; Ekeberg and Grillner, 1999) to understand the process of locomotion from nervous system to fluid, remains a key challenge for the future.

## ACKNOWLEDGMENTS

We thank all members of the Lauder Lab for many discussions regarding fish locomotion, especially Paul Webb and Bill Schultz for stimulating debate on the balance of thrust and drag. Kathy Dickson kindly supplied data on scombrid locomotion for Figure 11.1, and Jacquan Horton, Adam Summers, and Eliot Drucker provided data for Figure 11.3B. This research was supported by the National Science Foundation under grant IBN0316675 to G.V.L.

## REFERENCES

Aleev, Y. G. (1977). "Nekton." Junk Publishers, The Hague.

Anderson, E. J., McGillis, W. R., and Grosenbaugh, M. A. (2000). The boundary layer of swimming fish. *J. Exp. Biol.* **204,** 81–102.

Anderson, J. (1996). Vorticity control for efficient propulsion. Ph.D. thesis, MIT/WHOI

96–02.
Anderson, J. M., and Chhabra, N. (2002). Maneuvering and stability performance of a robotic tuna. *Integr. Comp. Biol.* **42,** 118–126.
Anderson, J. M., Streitlein, K., Barrett, D., and Triantafyllou, G. S. (1998). Oscillating foils of high propulsive efficiency. *J. Fluid Mech.* **360,** 41–72.
Arnold, G. P., Webb, P. W., and Holford, B. H. (1991). The role of the pectoral fins in station-holding of Atlantic salmon parr (*Salmo salar L.*). *J. Exp. Biol.* **156,** 625–629.
Arreola, V., and Westneat, M. W. (1997). Mechanics of propulsion by multiple fins: Kinematics of aquatic locomotion in the burrfish (*Chilomycterus schoepfi*). *Phil. Trans. Roy. Soc. Lond. B* **263,** 1689–1696.
Barrett, D., Triantafyllou, M. S., Yue, D. K. P., Grosenbaugh, M. A., and Wolfgang, M. J. (1999). Drag reduction in fish-like locomotion. *J. Fluid Mech.* **392,** 183–212.
Batchelor, G. K. (1973). "An Introduction to Fluid Mechanics." Cambridge Univ. Press, Cambridge, UK.
Blake, R. W. (1983). "Fish Locomotion." Cambridge Univ. Press, Cambridge, UK.
Bone, Q. (1978). Locomotor muscle. *In* "Fish Physiology. Vol. VII. Locomotion" (Hoar, W. S., and Randall, D. J., Eds.), pp. 361–424. Academic Press, New York.
Breder, C. M. (1926). The locomotion of fishes. *Zoologica N. Y.* **4,** 159–256.
Carling, J. C., Williams, T. L., and Bowtell, G. (1998). Self-propelled anguilliform swimming: Simultaneous solution of the two-dimensional Navier-Stokes equations and Newton's laws of motion. *J. Exp. Biol.* **201,** 3143–3166.
Castro-Santos, T. (2004). Quantifying the combined effects of attempt rate and swimming capacity on passage through velocity barriers. *Can. J. Fish. Aq. Sci.* **61,** 1602–1615.
Castro-Santos, T. (2005). Optimal swim speeds for traversing velocity barriers: An analysis of volitional high-speed swimming behavior of migratory fishes. *J. Exp. Biol.* **208,** 421–432.
Childress, S. (1981). "Mechanics of Flying and Swimming." Cambridge Univ. Press, Cambridge, UK.
Cortez, R., Fauci, L., Cowen, N., and Dillon, R. (2004). Simulation of swimming organisms: Coupling internal mechanics with external fluid dynamics. *Comp. Sci. Eng.* **6,** 38–45.
Daniel, T. L. (1984). Unsteady aspects of aquatic locomotion. *Amer. Zool.* **24,** 121–134.
Daniel, T. L., and Webb, P. W. (1987). Physics, design and locomotor performance. *In* "Comparative Physiology: Life in Water and on Land" (Dejours, P., Bolis, L., Taylor, C. R., and Weibel, E. R., Eds.), pp. 343–369. Liviana Press, Springer Verlag, New York.
Denny, M. W. (1993). "Air and Water. The Biology and Physics of Life's Media." Princeton Univ. Press, Princeton, NJ.
Dewar, H., and Graham, J. B. (1994). Studies of tropical tuna swimming performance in a large water tunnel. III. Kinematics. *J. Exp. Biol.* **192,** 45–59.
Donley, J., and Dickson, K. A. (2000). Swimming kinematics of juvenile Kawakawa tuna (*Euthynnus affinis*) and chub mackerel (*Scomber japonicus*). *J. Exp. Biol.* **203,** 3103–3116.
Donley, J., and Shadwick, R. (2003). Steady swimming muscle dynamics in the leopard shark *Triakis semifasciata*. *J. Exp. Biol.* **206,** 1117–1126.
Drucker, E. G., and Lauder, G. V. (2000). A hydrodynamic analysis of fish swimming speed: Wake structure and locomotor force in slow and fast labriform swimmers. *J. Exp. Biol.* **203,** 2379–2393.
Drucker, E. G., and Lauder, G. V. (2001a). Locomotor function of the dorsal fin in teleost fishes: Experimental analysis of wake forces in sunfish. *J. Exp. Biol.* **204,** 2943–2958.
Drucker, E. G., and Lauder, G. V. (2001b). Wake dynamics and fluid forces of turning maneuvers in sunfish. *J. Exp. Biol.* **204,** 431–442.
Ekeberg, Ö. (1993). A combined neuronal and mechanical model of fish swimming. *Biol.*

*Cybernet.* **69,** 363–374.
Ekeberg, Ö., and Grillner, S. (1999). Simulations of neuromuscular control in lamprey swimming. *Phil. Trans. Roy. Soc. Lond. B* **354,** 895–902.
Faber, T. E. (1995). "Fluid Dynamics for Physicists." Cambridge Univ. Press, Cambridge, UK.
Fauci, L. J., and Peskin, C. S. (1988). A computational model of aquatic animal locomotion. *J. Comp. Phys.* **77,** 85–108.
Ferry, L. A., and Lauder, G. V. (1996). Heterocercal tail function in leopard sharks: A three-dimensional kinematic analysis of two models. *J. Exp. Biol.* **199,** 2253–2268.
Fish, F., and Lauder, G. V. (2005). Passive and active flow control by swimming fishes and mammals. *Ann. Rev. Fluid Mech.* **38,** 193–224.
Geerlink, P. J., and Videler, J. (1974). Joints and muscles of the dorsal fin of *Tilapia nilotica* L. (Fam. Cichlidae). *Neth. J. Zool.* **24,** 279–290.
Gerstner, C. L., and Webb, P. W. (1998). The station-holding performance of the plaice *Pleuronectes platessa* on artificial substratum ripples. *Can. J. Zool.* **76,** 260–268.
Gillis, G. B. (1996). Undulatory locomotion in elongate aquatic vertebrates: Anguilliform swimming since Sir. James Gray. *Amer. Zool.* **36,** 656–665.
Gillis, G. B. (1998). Environmental effects on undulatory locomotion in the American eel *Anguilla rostrata*: Kinematics in water and on land. *J. Exp. Biol.* **201,** 949–961.
Gopalkrishnan, R., Triantafyllou, M. S., Triantafyllou, G. S., and Barrett, D. (1994). Active vorticity control in a shear flow using a flapping foil. *J. Fluid Mech.* **274,** 1–21.
Gosline, W. A. (1971). "Functional Morphology and Classification of Teleostean Fishes." Univ. of Hawaii Press, Honolulu, HI.
Graham, J. B., and Dickson, K. A. (2004). Tuna comparative physiology. *J. Exp. Biol.* **207,** 4015–4024.
Gray, J. (1933). Studies in animal locomotion. I. The movement of fish with special reference to the eel. *J. Exp. Biol.* **10,** 88–104.
Gray, J. (1936). Studies in animal locomotion. VI. The propulsive powers of the dolphin. *J. Exp. Biol.* **13,** 170–199.
Grillner, S. (2003). The motor infrastructure: From ion channels to neuronal networks. *Nat. Rev. Neurosci.* **4,** 573–586.
Haro, A., Castro-Santos, T., Noreika, J., and Odeh, M. (2004). Swimming performance of upstream migrant fishes in open-channel flow: A new approach to predicting passage through velocity barriers. *Can. J. Fish. Aq. Sci.* **61,** 1590–1601.
He, P., and Wardle, C. S. (1986). Tilting behavior of the Atlantic mackerel, *Scomber scombrus*, at low swimming speeds. *J. Fish. Biol.* **29,** 223–232.
Hertel, H. (1966). "Structure, Form and Movement." Reinhold, New York, NY.
Hess, F., and Videler, J. J. (1984). Fast continuous swimming of saithe (*Pollachius virens*): A dynamic analysis of bending moments and muscle power. *J. Exp. Biol.* **109,** 229–251.
Horton, J. M., Drucker, E., and Summers, A. (2003). Swiftly swimming fish show evidence of stiff spines. *Integ. Comp. Biol.* **43,** 905.
Hove, J. R., O'Bryan, L. M., Gordon, M. S., Webb, P. W., and Weihs, D. (2001). Boxfishes (Teleostei: Ostraciidae) as a model system for fishes swimming with many fins: Kinematics. *J. Exp. Biol.* **204,** 1459–1471.
Hover, F. S., Haugsdal, O., and Triantafyllou, M. S. (2004). Effect of angle of attack profiles in flapping foil propulsion. *J. Fluids Struct.* **19,** 37–47.
Hover, F. S., Techet, A. H., and Triantafyllou, M. S. (1998). Forces on oscillating uniform and tapered cylinders in crossflow. *J. Fluid Mech.* **363,** 97–114.
Jayne, B. C., and Lauder, G. V. (1995). Speed effects on midline kinematics during steady undulatory swimming of largemouth bass, *Micropterus salmoides*. *J. Exp. Biol.* **198,** 585–602.
Jayne, B. C., Lozada, A., and Lauder, G. V. (1996). Function of the dorsal fin in bluegill sunfish:

Motor patterns during four locomotor behaviors. *J. Morphol.* **228,** 307–326.
Lauder, G. V. (1982). Structure and function of the caudal skeleton in the pumpkinseed sunfish, *Lepomis gibbosus*. *J. Zool. (Lond.)* **197,** 483–495.
Lauder, G. V. (1989). Caudal fin locomotion in ray-finned fishes: Historical and functional analyses. *Amer. Zool.* **29,** 85–102.
Lauder, G. V. (2000). Function of the caudal fin during locomotion in fishes: Kinematics, flow visualization, and evolutionary patterns. *Amer. Zool.* **40,** 101–122.
Lauder, G. V. (2005). Locomotion. *In* "The Physiology of Fishes" (Evans, D. H., and Claiborne, J. B., Eds.). pp. 3–46. 3rd edn, CRC Press, Boca Raton, FL.
Lauder, G. V., and Drucker, E. (2002). Forces, fishes, and fluids: Hydrodynamic mechanisms of aquatic locomotion. *News Physiolog. Sci.* **17,** 235–240.
Lauder, G. V., and Drucker, E. G. (2004). Morphology and experimental hydrodynamics of fish fin control surfaces. *IEEE J. Oceanic Eng.* **29,** 556–571.
Lauder, G. V., Drucker, E. G., Nauen, J., and Wilga, C. D. (2003). Experimental hydrodynamics and evolution: Caudal fin locomotion in fishes. *In* "Vertebrate Biomechanics and Evolution" (Bels, V., Gasc, J.-P., and Casinos, A., Eds.), pp. 117–135. Bios Scientific Publishers, Oxford.
Lauder, G. V., Nauen, J., and Drucker, E. G. (2002). Experimental hydrodynamics and evolution: Function of median fins in ray-finned fishes. *Integr. Comp. Biol.* **42,** 1009–1017.
Lauder, G. V., and Tytell, E. D. (2004). Three Gray classics on the biomechanics of animal movement. *J. Exp. Biol.* **207,** 1597–1599.
Liao, J. (2004). Neuromuscular control of trout swimming in a vortex street: Implications for energy economy during the Karman gait. *J. Exp. Biol.* **207,** 3495–3506.
Liao, J., and Lauder, G. V. (2000). Function of the heterocercal tail in white sturgeon: Flow visualization during steady swimming and vertical maneuvering. *J. Exp. Biol.* **203,** 3585–3594.
Liao, J., Beal, D. N., Lauder, G. V., and Triantafyllou, M. S. (2003a). Fish exploiting vortices decrease muscle activity. *Science* **302,** 1566–1569.
Liao, J., Beal, D. N., Lauder, G. V., and Triantafyllou, M. S. (2003b). The Kármán gait: Novel body kinematics of rainbow trout swimming in a vortex street. *J. Exp. Biol.* **206,** 1059–1073.
Lighthill, J. (1960). Note on the swimming of slender fish. *J. Fluid Mech.* **9,** 305–317.
Lighthill, J. (1969). Hydromechanics of aquatic animal propulsion: A survey. *Ann. Rev. Fluid Mech.* **1,** 413–446.
Lighthill, J. (1970). Aquatic animal propulsion of high hydromechanical efficiency. *J. Fluid Mech.* **44,** 265–301.
Lighthill, J. (1971). Large-amplitude elongated body theory of fish locomotion. *Proc. Roy. Soc. Lond. B* **179,** 125–138.
Lindsey, C. C. (1978). Form, function, and locomotory habits in fish. *In* "Fish Physiology. Vol. VII. Locomotion" (Hoar, W. S., and Randall, D. J., Eds.), pp. 1–100. Academic Press, New York.
Liu, H. (2002). Computational biological fluid dynamics: Digitizing and visualizing animal swimming and flying. *Integr. Comp. Biol.* **42,** 1050–1059.
Liu, H., Wassersug, R. J., and Kawachi, K. (1996). A computational fluid dynamics study of tadpole swimming. *J. Exp. Biol.* **199,** 1245–1260.
Magnuson, J. J. (1978). Locomotion by scombrid fishes: Hydromechanics, morphology, and behavior. *In* "Fish Physiology. Vol. VII. Locomotion" (Hoar, W. S., and Randall, D. J., Eds.), pp. 239–313. Academic Press, New York.
McCutchen, C. W. (1977). Froude propulsive efficiency of a small fish, measured by wake visualization. *In* "Scale Effects in Animal Locomotion" (Pedley, T. J., Ed.), pp. 339–363.

Academic Press, London.
McLaughlin, R. L., and Noakes, D. L. G. (1998). Going against the flow: An examination of the propulsive movements made by young brook trout in streams. *Can. J. Fish. Aq. Sci.* **V55,** 853–860.
Mittal, R. (2004). Computational modeling in biohydrodynamics: Trends, challenges, and recent advances. *IEEE J. Oceanic Eng.* **29,** 595–604.
Müller, U. K., Smit, J., Stamhuis, E. J., and Videler, J. J. (2001). How the body contributes to the wake in undulatory fish swimming: Flow fields of a swimming eel (*Anguilla anguilla*). *J. Exp. Biol.* **204,** 2751–2762.
Müller, U. K., Stamhuis, E., and Videler, J. (2002). Riding the waves: The role of the body wave in undulatory fish swimming. *Integr. Comp. Biol.* **42,** 981–987.
Müller, U. K., Van den Heuvel, B., Stamhuis, E. J., and Videler, J. J. (1997). Fish foot prints: Morphology and energetics of the wake behind a continuously swimming mullet (*Chelon labrosus* Risso). *J. Exp. Biol.* **200,** 2893–2906.
Murray, M., and Howle, L. E. (2003). Spring stiffness influence of an oscillating propulsor. *J. Fluids Struct.* **17,** 915–926.
Nauen, J. C., and Lauder, G. V. (2001). Locomotion in scombrid fishes: Visualization of flow around the caudal peduncle and finlets of the Chub mackerel *Scomber japonicus*. *J. Exp. Biol.* **204,** 2251–2263.
Nauen, J. C., and Lauder, G. V. (2002a). Hydrodynamics of caudal fin locomotion by chub mackerel, *Scomber japonicus* (Scombridae). *J. Exp. Biol.* **205,** 1709–1724.
Nauen, J. C., and Lauder, G. V. (2002b). Quantification of the wake of rainbow trout (*Oncorhynchus mykiss*) using three-dimensional stereoscopic digital particle image velocimetry. *J. Exp. Biol.* **205,** 3271–3279.
Noca, F., Shiels, D., and Jeon, D. (1999). A comparison of methods for evaluating time-dependent fluid dynamic forces on bodies, using only velocity fields and their derivatives. *J. Fluids Struct.* **13,** 551–578.
Pedley, T. J. (1977). "Scale Effects in Animal Locomotion." Academic Press, London.
Raffel, M., Willert, C., and Kompenhans, J. (1998). "Particle Image Velocimetry: A Practical Guide." Springer-Verlag, Heidelberg.
Read, D. A., Hover, F. S., and Triantafyllou, M. S. (2003). Forces on oscillating foils for propulsion and maneuvering. *J. Fluids Struct.* **17,** 163–183.
Rohr, J., and Fish, F. (2004). Strouhal numbers and optimization of swimming by odontocete cetaceans. *J. Exp. Biol.* **207,** 1633–1642.
Rosen, M., Spedding, G. R., and Hedenstrom, A. (2004). The relationship between wingbeat kinematics and vortex wake of a thrush nightingale. *J. Exp. Biol.* **207,** 4255–4268.
Rosen, M. W. (1959). Water flow about a swimming fish. *Naval Ordnance Test Station.* Technical Paper. **2298,** 1–96.
Sakakibara, J., Nakagawa, M., and Yoshida, M. (2004). Stereo-PIV study of flow around a maneuvering fish. *Exp. Fluid* **36,** 282–293.
Schultz, W. W., and Webb, P. W. (2002). Power requirements for swimming: Do new methods resolve old questions? *Integr. Comp. Biol.* **42,** 1018–1025.
Standen, E. M., and Lauder, G. V. (2005). Dorsal and anal fin function in bluegill sunfish (*Lepomis macrochirus*): Three-dimensional kinematics during propulsion and maneuvering. *J. Exp. Biol.* **205,** 2753–2763.
Sutterlin, A. M., and Waddy, S. (1975). Possible role of the posterior lateral line in obstacle entrainment by Brook trout (*Salvelinus fontinalis*). *J. Fish. Res. Bd. Can.* **32,** 2441–2446.
Svendsen, J. C., Koed, A., and Lucas, M. C. (2005). The angle of attack of the body of common bream while swimming at different speeds in a flume tank. *J. Fish. Biol.* **66,** 572–577.
Taylor, G. I. (1952). Analysis of the swimming of long and narrow animals. *Proc. Roy. Soc.*

*Lond. A* **214,** 158–183.
Taylor, G. K., Nudds, R. L., and Thomas, A. (2003). Flying and swimming animals cruise at a Strouhal number tuned for high power efficiency. *Nature* **425,** 707–711.
Triantafyllou, M. S., and Triantafyllou, G. S. (1995). An efficient swimming machine. *Sci. Am.* **272,** 64–70.
Triantafyllou, G. S., Triantafyllou, M. S., and Grosenbaugh, M. A. (1993). Optimal thrust development in oscillating foils with application to fish propulsion. *J. Fluids Struct.* **7,** 205–224.
Triantafyllou, M. S., Techet, A. H., and Hover, F. S. (2004). Review of experimental work in biomimetic foils. *IEEE J. Oceanic Eng.* **29,** 585–594.
Tytell, E. D. (2004a). The hydrodynamics of eel swimming II. Effect of swimming speed. *J. Exp. Biol.* **207,** 3265–3279.
Tytell, E. D. (2004b). Kinematics and hydrodynamics of linear acceleration in eels, *Anguilla rostrata*. *Proc. Roy. Soc. Lond. B* **271,** 2535–2540.
Tytell, E. D., and Lauder, G. V. (2004). The hydrodynamics of eel swimming. I. Wake structure. *J. Exp. Biol.* **207,** 1825–1841.
Veerman, H. P., and Den Boer, R. (2000). PIV measurements in presence of a large out of plane component. *In* "Particle Image Velocimetry. Progress toward Industrial Application" (Stanislas, M., Kompenhans, J., and Westerweel, J., Eds.), pp. 217–225. Kluwer Academic, Dordrecht.
Videler, J. J. (1993). "Fish Swimming." Chapman and Hall, New York.
Videler, J. J., and Hess, F. (1984). Fast continuous swimming of two pelagic predators, saithe (*Pollachius virens*) and mackerel (*Scomber scombrus*): A kinematic analysis. *J. Exp. Biol.* **109,** 209–228.
Webb, P. W. (1975). Hydrodynamics and energetics of fish propulsion. *Bull. Fish. Res. Bd. Can.* **190,** 1–159.
Webb, P. W. (1978). Hydrodynamics: Nonscombroid fish. *In* "Fish Physiology. Vol. VII. Locomotion" (Hoar, W. S., and Randall, D. J., Eds.), pp. 189–237. Academic Press, New York.
Webb, P. W. (1991). Composition and mechanics of routine swimming of rainbow trout, *Oncorhynchus mykiss*. *Can. J. Fish. Aquat. Sci.* **48,** 583–590.
Webb, P. W. (1993a). Is tilting behavior at low speed swimming unique to negatively buoyant fish? Observations on steelhead trout, *Oncorhynchus mykiss*, and bluegill, *Lepomis macrochirus*. *J. Fish. Biol.* **43,** 687–694.
Webb, P. W. (1993b). Swimming. *In* "The Physiology of Fishes" (Evans, D. H., Ed.), pp. 47–73. CRC Press, Boca Raton, FL.
Webb, P. W. (1998). Entrainment by river chub *Nocomis micropogon* and smallmouth bass *Micropterus dolomieu* on cylinders. *J. Exp. Biol.* **201,** 2403–2412.
Webb, P. W., and Blake, R. W. (1985). Swimming. *In* "Functional Vertebrate Morphology" (Hildebrand, M., Bramble, D. M., Liem, K. F., and Wake, D. B., Eds.), pp. 110–128. Harvard Univ. Press, Cambridge, MA.
Webb, P. W., and Keyes, R. S. (1981). Division of labor between median fins in swimming dolphin (Pisces: Coryphaenidae). *Copeia* **1981,** 901–904.
Webb, P. W., and Weihs, D. (1983). "Fish Biomechanics." Praeger Publishers, New York.
Weihs, D. (1972). A hydrodynamic analysis of fish turning manoeuvres. *Proc. Roy. Soc. Lond. B* **182B,** 59–72.
Westerweel, J., and Oord, J.v. (2000). Stereoscopic PIV measurements in a turbulent boundary layer. *In* "Particle Image Velocimetry. Progress toward Industrial Application" (Stanislas, M., Kompenhans, J., and Westerweel, J., Eds.), pp. 459–478. Kluwer Academic, Dordrecht.
Wilga, C. D., and Lauder, G. V. (1999). Locomotion in sturgeon: Function of the pectoral fins.

*J. Exp. Biol.* **202,** 2413–2432.

Wilga, C. D., and Lauder, G. V. (2000). Three-dimensional kinematics and wake structure of the pectoral fins during locomotion in leopard sharks *Triakis semifasciata*. *J. Exp. Biol.* **203,** 2261–2278.

Wilga, C. D., and Lauder, G. V. (2002). Function of the heterocercal tail in sharks: Quantitative wake dynamics during steady horizontal swimming and vertical maneuvering. *J. Exp. Biol.* **205,** 2365–2374.

Wilga, C. D., and Lauder, G. V. (2004). Hydrodynamic function of the shark's tail. *Nature* **430,** 850.

Willert, C. (1997). Stereoscopic digital particle image velocimetry for application in wind tunnel flows. *Meas. Sci. Technol.* **8,** 1465–1479.

Willert, C. E., and Gharib, M. (1991). Digital particle image velocimetry. *Exp. Fluid* **10,** 181–193.

Williams, T. L., Bowtell, G., Carling, J. C., Sigvardt, K. A., and Curtin, N. A. (1995). Interactions between muscle activation, body curvature and the water in the swimming lamprey. *In* "Biological Fluid Dynamics" (Ellington, C. P., and Pedley, T. J., Eds.), pp. 49–59. Company of Biologists, Cambridge.

Winterbottom, R. (1974). A descriptive synonymy of the striated muscles of the Teleostei. *Proc. Acad. Nat. Sci. Phila.* **125,** 225–317.

Wolfgang, M. J., Anderson, J. M., Grosenbaugh, M., Yue, D., and Triantafyllou, M. (1999). Near-body flow dynamics in swimming fish. *J. Exp. Biol.* **202,** 2303–2327.

Wu, Y. T. (1971). Hydromechanics of swimming propulsion. Part I. Swimming of a two-dimensional flexible plate at variable forward speeds in an inviscid fluid. *J. Fluid Mech.* **46,** 337–355.

Zhu, Q., Wolfgang, M. J., Yue, D. K. P., and Triantafyllou, G. S. (2002). Three-dimensional flow structures and vorticity control in fish-like swimming. *J. Fluid Mech.* **468,** 1–28.